Nanoscale heterogeneity, premartensitic nucleation, and a new plutonium structure in metastable δ fcc Pu-Ga alloys

Steven D. Conradson,[1,*] Nicolas Bock,[2] Julio M. Castro,[3] Dylan R. Conradson,[2] Lawrence E. Cox,[4] Wojciech Dmowski,[5] David E. Dooley,[4] Takeshi Egami,[5] Francisco J. Espinosa-Faller,[6] Franz J. Freibert,[1] Angel J. Garcia-Adeva,[7] Nancy J. Hess,[8] Erik K. Holmström,[2] Rafael C. Howell,[1] Barbara Katz,[4] Jason C. Lashley,[1] Raymond J. Martinez,[1] David P. Moore,[1] Luis A. Morales,[1] J. David Olivas,[1] Ramiro A. Pereyra,[4] Michael Ramos,[1] Sven P. Rudin,[2] and Phillip M. Villella[1]

[1]*Materials Science and Technology Division, Los Alamos National Laboratory, Los Alamos, New Mexico 87545, USA*
[2]*Theoretical Division, Los Alamos National Laboratory, Los Alamos, New Mexico 87545, USA*
[3]*Health, Safety, Radiation Protection Division, Los Alamos National Laboratory, Los Alamos, New Mexico 87545, USA*
[4]*Nuclear Materials Technology Division, Los Alamos National Laboratory, Los Alamos, New Mexico 87545, USA*
[5]*Department of Physics and Astronomy, University of Tennessee, Knoxville, Tennessee 37996, USA*
[6]*Departamento de Física para Ingenieros, Universidad Marista de Merida, Merida, Yucatan 97300, Mexico*
[7]*Departamento de Fisica Aplicada I, E.T.S. Ingenieria de Bilbao, Universidad del Pais Vasco, Alda. Urquijo s/n, 48013 Bilbao, Spain*
[8]*Environmental Molecular Sciences Laboratory, Pacific Northwest National Laboratory, Richland, Washington 99352, USA*

The scientifically fascinating question of the spatial extent and bonding of the $5f$ orbitals of Pu and its six different phases extends to its δ-retained alloys and the mechanism by which Ga and a number of other unrelated elements stabilize its low density face-centered-cubic (fcc) structure. This issue of phase stability is also important technologically because of its significance to Science-Based Stockpile Stewardship. Answering these questions requires information on the local order and structure around the Ga and its effects on the Pu. We have addressed this by characterizing the structures of a large number of Pu-Ga and two Pu-In and one Pu-Ce δ alloys, including a set of high purity δ $Pu_{1-x}Ga_x$ materials with $1.7 \leq x \leq 6.4$ at. % Ga that span the low [Ga] portion of the δ region of the phase diagram across the ∼3.3 at. % Ga metastability boundary, with extended x-ray absorption fine structure (EXAFS) spectroscopy that probes the element specific local structure, supplemented by x-ray pair distribution function analysis that gives the total local structure to longer distances, and x-ray diffraction that gives the long-range average structure of the periodic component of the materials. Detailed analyses indicate that the alloys at and below a nominal composition of ∼3.3 at. % Ga are heterogeneous and in addition to the δ phase also contain up to ∼20% of a novel, coexisting "σ" structure for Pu that forms in nanometer scale domains that are locally depleted in Ga. The invariance of the Ga EXAFS with composition indicates that this σ structure forms in Ga-depleted domains that result from the Ga atoms in the δ phase self-organizing into a quasi-intermetallic with a stoichiometry of $Pu_{25-35}Ga$ so that δ Pu-Ga is neither a random solid solution nor the more stable $Pu_3Ga + \alpha$. Above this 3.3 at. % Ga nominal composition, the δ Pu-Ga alloy is homogeneous, and no σ phase is present. These results that demonstrate that collective and cooperative behavior in the interactions between the alloy elements as well as local elastic forces are crucial in determining the properties of complex materials and contradict the conventional mechanism for martensitic transformations, in this case indicating that nucleation is not the rate limiting step.

PACS number(s): 61.05.cj, 61.05.cf, 61.46.−w, 61.66.Dk

I. INTRODUCTION

Plutonium (Pu) is by consensus the most astonishing member of the actinides [1–6], the class of the elements in which the $5f$ electron shell is progressively filled. The heavier members of the actinide series (Am, Cm, and beyond) have larger atomic volumes that are almost independent of the $5f$ electron population. This behavior resembles those of the lanthanide elements; the $5f$ states are localized and do not participate in the bonding. In contrast, in the early part of this series (Th, Pa, U, and Np), the spatially extended $5f$ electrons contribute to the bonding between atoms to give high density materials with short interatomic distances. The $5f$ participation in bonding results in an atomic volume dependence on electron population similar to that of the transition metal series. In Pu, the $5f$ electrons are "on the edge"

[3–5,7–15], and it is this unique $5f$ configuration that gives this element a host of unusual properties. Since the discovery of Pu in 1941, the element's eccentricities have both awed and perplexed researchers [2,16]. Understanding its properties is indeed critical for the safe handling, use [17,18], and long-term storage of this highly toxic, radioactive, but technologically important material [2,16].

The complex and often unique properties of Pu have been well documented [19], especially with its recent renaissance in which the technology drivers of stockpile stewardship [2,16–18] have stimulated intense investigation of the scientific issues [2–6]. The pure metal exhibits six solid-state phases with large volume expansions and subsequent contractions along the way to melting at a relatively low ∼650 °C to yield a higher density liquid than that of the solid from which it derives [2,4,19]: α (monoclinic) → β (monoclinic) → γ (orthorhombic) → δ (face-centered-cubic [fcc]) → δ′ (face-centered-tetragonal [fct]) → ε (body-centered-cubic [bcc]) → liquid. There have also, however, been reports and suggestions of nanophase

―――――――

*Corresponding author: conradson@lanl.gov

formation of these, related, or even novel structures in response to local, intracrystal composition fluctuations in alloys or the lowered dimensionality of surfaces [20–25]. The fcc δ phase with density ~15.8 g/cc is 20% lower in density than the monoclinic α phase (19.86 g/cc). This fcc δ phase when stabilized or retained by alloying has desirable mechanical properties such as ductility that allow it to be formed into complicated shapes and is thus the most technologically important structure. The monoclinic α phase, on the other hand, is quite brittle and difficult to machine.

To overcome these engineering challenges, Pu can be stabilized or retained in the δ phase by alloying with Group III metals such as Al and Ga but also others like Ce and Am and even nonmetallic elements like Si. The list of δ stabilizers fails to clarify the stabilization mechanism. Some are trivalent, others are not, some are larger than Pu, others smaller, some are more electropositive, others more electronegative, so that there is no obvious common characteristic. The different elements have vastly different ranges of δ stabilization/retention to room temperature and below [19]. The stabilization is not simply a shifting of the transition temperatures; the transformation that can be induced by cooling or pressure in alloys with δ stabilizers below certain thresholds takes the (metastable at these compositions) δ phase directly to the α' one ($\alpha' =$ impure α Pu with small distortions) by a martensitic mechanism [26]. Kinetic trapping is quite common so that the δ phase is often easily obtained well outside the compositions of the phase boundaries, which are therefore difficult to establish precisely. The accumulation of residual stress in the micron-scale grains of material stops the $\delta \rightarrow \alpha$ martensitic transformation process that is induced by cooling after a few dozen percent have transformed and also causes the reverse transformation to occur via a regular pattern of bursts [5,19,27–31]. Retention of the δ phase to room temperature and below by alloying while retaining the nuclear and engineering properties of Pu is the metallurgical challenge [2,5,6,19].

Ga is one of the most technologically important δ stabilizers, although barring new or more complete data, consensus has recently been reached that Ga retains rather than stabilizes the δ phase with respect to its very slow phase separation into a more thermodynamically stable mixture of α Pu and Pu_3Ga [5]. Phase pure (by diffraction) Pu-Ga alloys exhibit the δ structure at room temperature from as low as 1 at. % with careful annealing to around 10–12.5 at. %, after which they separate into δ Pu $+$ Pu_3Ga [5,19]. The addition of the 4% smaller Ga atoms [19,25,32–36] causes the lattice to contract, from $a = 4.64$ Å in pure δ Pu to 4.56 Å at 9.9 at. % Ga and 4.51 Å in Pu_3Ga [2,19]. Here, δ Pu-Ga alloys are metastable with respect to the pressure- and temperature-induced martensitic transformation to α' Pu below about 3.3 at. % Ga [5,19]. We have previously reported on radical behavior of the local structure correlated with these transformational properties [20,21,37] that has since been corroborated in an Al alloy by x-ray pair distribution function (PDF) measurements [24] and in Pu-Ga by extended x-ray absorption fine structure (EXAFS) spectroscopy [25].

In this paper, we show x-ray scattering and EXAFS measurements of a number of δ Pu-Ga samples culminating with a series of high purity Pu-Ga alloys made systematically

from zone-refined Pu as a function of Ga content in the range 1.7 to 6.5 at. % Ga. The results were analyzed in some detail to gain insight into the nature of the microstructure, homogeneity, and phases in these intriguing binary alloys of plutonium. This set of local structure measurements probing the element specific environments below the diffraction limit [20,38–44] demonstrates that, far from being a random solid solution, the behavior of the Ga atoms is totally dissimilar to the Pu. The Ga atoms that rigorously avoid bonding to each other even at relatively high concentrations nevertheless interact over longer distances so that they are loosely organized into a quasi-intermetallic. At compositions below the level where this intermetallic saturates the crystal, the Pu atoms in the Ga-depleted regions rearrange into a structure that is not one of the known Pu phases and is therefore novel. Above the saturation level, the Ga local environments are conserved even as the preferred structure is disrupted by the additional Ga, forcing all of the local strain into the Pu environments that respond by forming additional types of locally ordered lattice distortions.

II. EXPERIMENTAL AND ANALYTICAL METHODS

Pu and its compounds are toxicological and radiological hazards and can only be handled in special facilities by trained personnel. Pu metal and alloys are readily oxidized in air, and the resulting surface oxide is quite friable so that it must be contained to avoid possible inhalation. At the synchrotron facilities, the Pu was protected within especially designed sample cells and laboratories with three independent levels of containment at all times and the airflow around the samples controlled and exhausted through high efficiency particulate air (HEPA) filters and surveyed with continuous air monitors.

X-ray absorption fine structure and x-ray diffraction (XRD) measurements reported here were performed over the course of 10 years on several sets of Pu-Ga and other alloys with various pedigrees that differed primarily in the numbers and concentrations of contaminants. The other critical process in the preparation of Pu alloys is the annealing that redistributes the Ga evenly within the grains after their growth from the melt through multiple phases that results in "coring" where the Ga is preferentially deposited in the centers of the grains and depleted on the edges. Samples for the experiments were mechanically rolled from cast buttons, annealed for a minimum of 48 h at 450–460 °C to give pure δ phase Pu-Ga with a homogeneous Ga distribution, cut to the correct size, mechanically polished to 100–200 μm thickness, electropolished to remove surface oxide and α Pu created during the polishing process, and then mounted within the nested sample holders that were filled with inert gas. All primary and secondary holders were checked for contamination prior to shipping to the synchrotron. Laboratory XRD measurements confirmed the compositions of many of the samples after preparation. Two of the samples (designated with an asterisk in the text and figures) contained a few tenths of a percent each of Pb and Sn that had only negligible effects on the structure and phase stability. X-ray absorption fine structure measurements on these initial samples were performed at either ~80 K by mounting the holder to the cold finger of a liquid nitrogen reservoir-type cryostat or at 25–40 K using an open cycle

liquid He refrigeration system. The $Pu_{0.973}Ga_{0.027}$ sample used for x-ray PDF analysis (and EXAFS) was prepared from electrorefined Pu and annealed for 200 h. Another sample used for PDF is aged $Pu_{0.9983}Ga_{0.017}$ material; aging processes are outside the scope of this report (although included in a companion paper [37]), but this sample was sufficiently young that its structure is almost identical to that of new samples. This study culminated in a suite of six alloys with 1.7, 2.3, 3.0, 3.7, 4.7, and 6.5 at. % Ga, prepared by arc melting Ga and Pu that had been purified by zone refining to bring all contaminants down to a few tens of parts per million or less with the exception of U that was around 100–120 ppm [31,45]. These alloys were made by arc melting the Pu and Ga, rolling, and annealing for 48 h at 450 °C, at which time all traces of α Pu were eliminated from the diffraction pattern in the most sensitive $Pu_{0.983}Ga_{0.017}$ sample as well as the others. This was subsequently confirmed by extensive diffraction measurements on several samples at the synchrotron across a temperature range of 10–140 K. Pu XAFS measurements on these samples were made at 35, 90, and 300 K, Ga XAFS measurements on all samples were performed at 300 K, but because of the exigencies of beam time only the 1.7, 3.0, 4.7, and 6.5 at. % Ga samples at 35 and 90 K. No evidence of any oxide or other surface contaminant affecting the data was found by XRD or within the EXAFS for these samples because the depth of penetration is much greater than that from a Cu x-ray tube in the laboratory.

Experimental measurements were performed at the Stanford Synchrotron Radiation Laboratory on end stations 4-2, 7-2, and 11-2. Si [220] monochromator crystals were fully tuned with harmonic rejection for XAFS accomplished with a flat, Pt-coated mirror tilted to have a cutoff energy of 21–25 keV for Pu and 13–15 keV for Ga and unnecessary at the 30 keV energies of the scattering measurements. The energy was calibrated by defining the first inflection point of a Zr foil as 17 999.35 eV, which puts the inflection point of the Pu edge at 18 056.7–18 057.0 eV. Useful EXAFS spectra were obtained near 35 and 85 K because of the low Debye temperature of δ Pu [35]. Ambient temperature measurements were also made prior to cooling, with sufficient data quality to confirm that no significant changes in the samples were induced by the temperature change [20,21,37]. The temperature-induced martensitic transformation to $\alpha-\delta$ mixtures has not been observed in EXAFS [20,32–36,46,47] or x-ray/neutron scattering [23,48] measurements on such samples—including those presented here, although broadening of the Bragg peaks does occasionally occur. Other types of measurements, however, have found evidence for complicated transformational behavior extending to very low temperatures [49,50] that therefore, by definition, involve the formation of poorly diffracting and nondiffracting domains associated with the retained δ precursor and host. Results reported here corroborate this idea of the transformation mechanism involving more than just a shifting of micron-sized domains of atoms between the α and δ phases and will perhaps help clarify this conundrum.

Extended x-ray absorption fine structure measurements were made in the fluorescence mode. When using a multi-element Ge detector, count rates in each detector channel were kept below 120 kHz so that all live times exceed 0.9, and the corrections made using 1.0–1.5 μsec dead times were small. Samples were >100 μm thick to avoid possible artifacts that could result from fabricating Pu foils <20 μm. Insofar as the analyses as performed are based on direct comparisons of the spectra of these fully absorbing samples, self-absorbance corrections were unnecessary and were not performed. The resulting error is <1% because of the low Ga concentration and especially because the increase in Ga concentration is coincidentally almost exactly cancelled by the concomitant decrease in the lattice constant. The x-ray PDF measurements were performed in reflection geometry at 33 keV.

Extended x-ray absorption fine structure and x-ray PDF data were analyzed using our own software package that we apply routinely to actinide systems [51,52], with great care taken in the analysis and especially the EXAFS normalization and background subtraction to use very similar spline parameters for all spectra so that differences between them cannot be analysis artifacts. The EXAFS were calculated as the difference between the full spectra and their smooth atomic backgrounds approximated by an arctangent and Gaussian for the edge and a polynomial spline at higher energies, divided by the atomic absorbance fall off with increasing energy. The locations of the spline knots were varied to minimize the modulus area below $R = 2$ Å, with the caveat that the general locations were similar for all spectra. The lower limit of useful data for the older samples was set at $k \sim 5.2$ Å^{-1} so that less time had to be spent determining accurate, consistent backgrounds through the region where the Ramsauer-Townsend effect produces a beat in the EXAFS. The upper limit of 12–13 Å^{-1} was set by this being the high end for a few samples that were nevertheless important in the comparisons, with the high quality samples analyzed over a much wider range 3.7–15.85 Å^{-1}. Spectra that were used more extensively cover a greater range. Curve-fits using amplitudes and phases calculated with the FEFF code [53] allowed the number of atoms (N), σ (the Gaussian width of the pairwise harmonic distribution), r (interatomic distance) to float, with the $\Delta E_0 s$ constrained to be equal for all shells and typically constrained and fixed σ values for the more distant shells to obtain reasonable values for N. Metrical parameters obtained from the curve-fitting are reported (Table I), although not used much in the interpretation except for some of the distances since, as these experiments demonstrate and as this paper will describe, the materials are extensively disordered in complicated ways. Insofar as it appears that none of the materials can be described as possessing a homogeneous fcc structure, assigning the number 12 to the nearest neighbor δ shell at 3.28 Å as the basis for obtaining the numbers of neighbors in the other spectra is only approximate; only relative amounts are of any value. The purpose of the fits was to isolate the nearest neighbor contributions by subtracting those from other shells from the spectra and to identify non-δ structural features by similarly subtracting the fit with only the δ shells. These were subsequently used in the more direct amplitude ratioing/phase difference and amplitude integration or simply presented for direct comparison. While sacrificing some of the quantification accruing to curve-fits, these procedures nevertheless allow a higher degree of confidence in the results reported here whose focus is the presence of non-δ structures and other types of disorder.

TABLE I. Interatomic distances from curve-fits for high quality sample suite at 35 K. Disorder shortens bond lengths found by curve-fit.

δ Pu xtal		3.281 Å		4.640 Å	5.683 Å	6.562 Å	7.336 Å
Pu-Pu distances							
1.7 at. % Ga	2.655 ± 0.020	3.279 ± 0.009		4.624 ± 0.022	5.680 ± 0.014	6.541 ± 0.014	7.318 ± 0.019
2.3 at. % Ga		3.275 ± 0.009	3.800 ± 0.013	4.604 ± 0.020	5.661 ± 0.012	6.531 ± 0.013	7.289 ± 0.014
2.7 at. % Ga		3.286 ± 0.009	3.776 ± 0.012	4.616 ± 0.024	5.678 ± 0.012	6.552 ± 0.014	7.289 ± 0.013
3.0 at. % Ga		3.275 ± 0.010	3.803 ± 0.014	4.589 ± 0.028	5.663 ± 0.013	6.519 ± 0.014	7.227 ± 0.030
3.7 at. % Ga	2.817 ± 0.026	3.277 ± 0.010		4.605 ± 0.015	5.654 ± 0.014	6.523 ± 0.013	7.298 ± 0.014
4.7 at. % Ga	2.835 ± 0.019	3.279 ± 0.012		4.621 ± 0.015	5.663 ± 0.015	6.519 ± 0.014	7.252 ± 0.022
6.5 at. % Ga	2.821 ± 0.019	3.269 ± 0.014		4.549 ± 0.017	5.637 ± 0.028	6.497 ± 0.016	7.253 ± 0.027
Ga-Pu distances							
δ Pu xtal		3.281 Å		4.640 Å	5.683 Å		
1.7 at. % Ga		3.158 ± 0.014		4.603 ± 0.015	5.654 ± 0.015		
3.0 at. % Ga		3.157 ± 0.013		4.603 ± 0.015	5.641 ± 0.018		
4.7 at. % Ga		3.156 ± 0.012		4.589 ± 0.014	5.642 ± 0.016		
6.5 at. % Ga		3.150 ± 0.012		4.578 ± 0.014	5.635 ± 0.019		

III. RESULTS AND DISCUSSION

A. Evidence from high energy x-ray diffraction for the coexistence with δ Pu-Ga of a σ structure

Because Pu metal is so reactive, multiphase diffraction patterns using Cu laboratory x-ray sources are the rule rather than the exception since, unless extraordinary care is taken, the surface is coated with the various oxides and carbides that Pu forms. Our first observation of diffraction using higher energy synchrotron x-rays was how relatively clean the patterns were because the more highly penetrating x-rays were insensitive to the thin layer of surface contamination. Wide angle x-ray scattering data at 18 (just below the Pu L_3 absorption edge) or >30 keV were obtained on many samples at the synchrotron, with those from the 1.3*, 2.7, 2.7*, and aged 1.7 at. % Ga materials shown here (Fig. 1). The δ Pu-Ga *Fm3m* diffraction pattern [54], albeit exhibiting relative peak heights that are altered by texture in the samples, in all cases accounts for the most prominent diffraction peaks. The δ lattice constants are 4.6444, 4.6302, 4.6013, and 4.6230 Å for, respectively, the 1.3*, 1.7 aged, 2.7, and 2.7* at. % Ga samples at the indicated temperatures. Insofar as the Pb and Sn in the * samples slightly expand the lattice relative to more pure alloys, these values are consistent with their compositions and the temperature dependence of the Pu-Ga system [33]. The absence of the α Pu diffraction pattern indicates that, crystallographically, none of these materials underwent the partial transformation to α Pu on cooling [23]. This conundrum is common to all microstructure measurements and suggests that the martensitic transformation mechanism is more complicated than the assumed concerted, simple displacements of all of the atoms within micron scale domains [55].

In addition to the δ pattern and occasional extraneous Cu and Al peaks from the sample holder, the structure factors from the 1.3*, 2.7, and 2.7* at. % Ga δ Pu alloys at low temperature display another set of minor peaks that are not observed from the aged $Pu_{0.983}Ga_{0.017}$ sample (but whose PDF, discussed in a following section, nevertheless demonstrates that a second structure is present even when this diffraction pattern does not occur). These second diffraction patterns all index to

a second, 7% larger *Fm3m* structure with lattice constants of 4.9791 (1.3*), 4.9461 (2.7), and 4.9588 Å (2.7*). This pattern is often observed in the laboratory measurements with
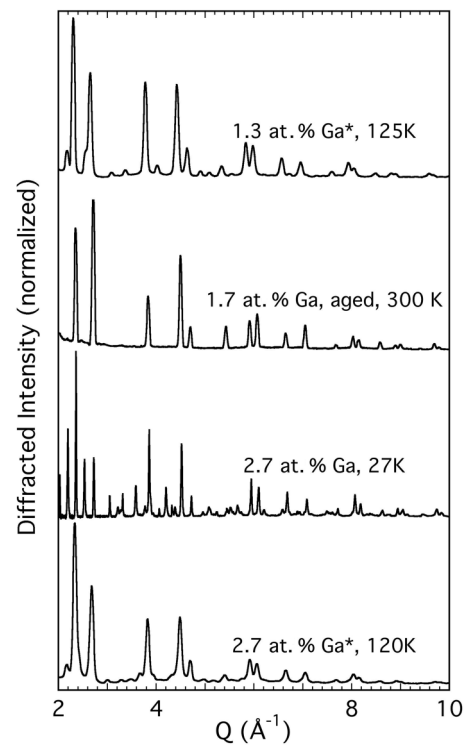

FIG. 1. X-ray diffraction patterns from three new and one aged Pu-Ga (* = the samples containing negligible amounts of Pb and Sn as described in the experimental section). Although the relative intensities of the diffraction peaks can differ because of texture (preferred grain orientations) in some samples, all these δ Pu-Ga alloy samples display the $Fm3m/a = 4.60$–4.64 Å diffraction pattern shifted to higher Q/lower a values with higher Ga concentrations that is characteristic of δ Pu. Close inspection of the baseline region reveals additional small peaks in the scattering profiles of the new Pu-Ga samples that constitute a second *Fm3m* diffraction pattern shifted to lower Q (larger lattice constant).
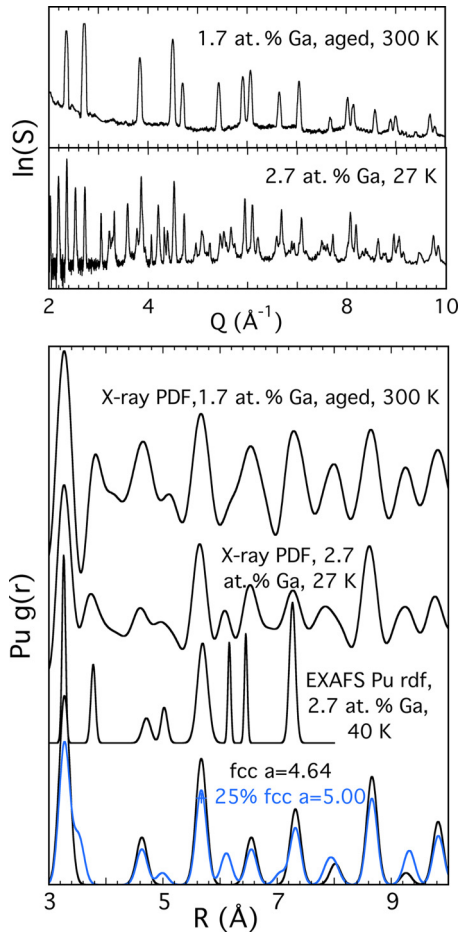
FIG. 2. (Color online) (Upper) Diffraction patterns of indicated samples showing the single diffraction pattern for the 1.7 at. % Ga aged sample and multiple patterns for the 2.7 at. % Ga new sample. The logarithm emphasizes the absence or presence of the second patterns. (Lower) Experimental pair distribution functions from these same aged (top) and new (second from top) Pu-Ga samples and calculated from the curve-fit of its Pu EXAFS spectrum (distances and relative peak areas are correct), and the calculated PDFs for the $Fm3m$, $a = 4.64$ δ Pu (lower trace, black) and the sum of this plus one-fourth as much of a second $Fm3m$, $a = 5.00$ Å structure (lower trace, blue in online version). Almost all of the features observed experimentally are accounted for by the composite of these two cubic structures, both when the multiple diffraction patterns are observed from the 2.7 at. % Ga sample and when only a single pattern occurs as from the 1.7 at. % Ga sample. All of the features of the model PDF also appear in the data, with the exception being the peak at 3.8 Å in the data that most likely corresponds to the calculated 3.5 Å peak after the structural modulation depicted in Fig. 3.

enhanced surface sensitivity, where it has commonly and often correctly been assigned to PuO(C) (plutonium oxycarbide) surface contamination [56,57]. The first two of these constants are, in fact, just outside of the range found for PuO(C) [56]. However, we interpret these measurements with sample penetration depths of 10 μm or more as indicating a second, coexisting, previously undescribed, cubic/fcc structure that we call "σ" because the combined evidence from diffraction, PDF (Fig. 2), and EXAFS (Fig. 3, etc.) overwhelmingly supports a
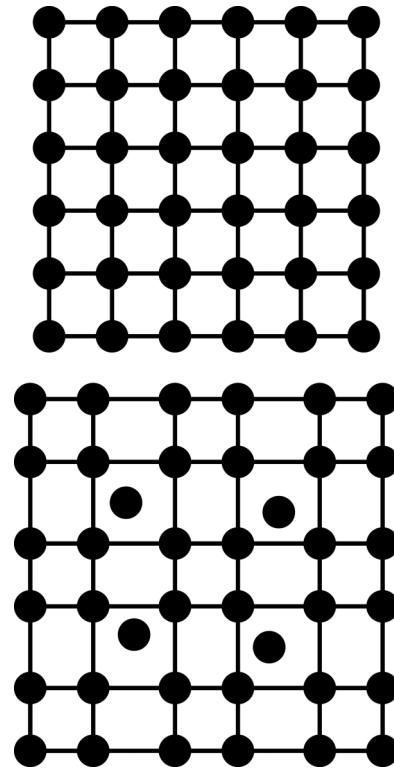

FIG. 3. An arrangement of atoms in two dimensions that gives the experimental results found for the σ structure is created analogously to this treatment of the square lattice (upper). A modulated pattern that averages to larger squares while retaining some of the original nearest neighbor distances results from expanding alternating squares along diagonals (lower). The original density is maintained by inserting disordered interstitials into the large squares that will give a broad peak in the distribution that will be invisible to EXAFS and unobservable in PDF data.

novel metallic structure as well as giving some characteristics of this putative σ Pu:

(a) This pattern cannot have originated in a surface contaminant or strain because the amplitudes of the diffraction peaks do not diminish as the penetration depth normal to the surface increases with increasing angle, nor does the EXAFS reflect a larger amount of this second phase consistent with its much smaller sampling depth.

(b) PuO(C) has never, to our knowledge, been described as a bulk contaminant of Pu with a uniform distribution over a depth of dozens of microns [57], nor is its formation coupled to the Ga concentration of the alloy, as will be described.

(c) These patterns were not observed at ambient temperature in identical 1.3* and 2.7* at. % Ga samples cut from the same button of material nor in the 1.7 at. % Ga aged sample, although PDF and EXAFS show that the σ structure is still present near 300 K in equal or comparable amounts as at 100 K and below and appears to be thermally harder rather than softer than δ Pu-Ga [37]. This indicates that the intradomain ordering and interdomain coherence of these nanodomains can be sensitive to the temperature even while the local ordering is not, which is not a characteristic of PuO(C). The PDF and EXAFS for Ga $\leq$ 3.3 at. % always show the local structure

indicative of σ Pu even when the *Fm*3*m* $a = 5.0$ Å diffraction pattern is not observed.

(d) The PDF and EXAFS show a prominent 3.8 Å Pu-Pu distance but not the 3.5 Å one expected for PuO(C) [recent XAFS measurements not shown here on Pu samples prepared so as to contain large amounts of PuO(C) in the top several μm show a completely different type of spectrum with the Pu-Pu distance near 3.5 Å] since all of the binary oxides of Pu studied show only a disordered single site distribution for the Pu-Pu pairs.

(e) The EXAFS does not show any evidence for the expected O/C nearest neighbors in association with the principal 3.8 Å Pu-Pu distance of the component despite the fact that their relative contribution should be especially large at higher temperatures [37] and in the low k data.

(f) Unusual ordering vis-á-vis the δ Pu is suggested by the poor correlation between the intensity of the diffraction peaks relative to the δ pattern and the amount of σ Pu indicated in the EXAFS and PDF.

(g) Intimate association with the Pu is demonstrated by the fact that, as a for these samples decreases by 0.033 Å with increasing Ga concentration, the difference between the δ and σ lattice parameters, $\Delta a(\delta - \sigma)$, < 0.008 Å is within the error level, a remarkable coincidence if there are not rigorous epitaxial constraints between the two structures that would not be the case of PuO(C) inclusions.

Although a more detailed discussion of the PDF and EXAFS continues below, given this list of evidence it will be done principally in the context that Pu-Ga alloys frequently do exhibit nanoscale heterogeneity [40] in the form of a δ host lattice that contains up to $\sim 20\%$ of a second, ordered σ structure residing in embedded domains that are intimately associated with the host but whose size and coherence are at or below the diffraction limit [20]. The label "structure" is perhaps preferable to "phase" because it has only been found as nanoscale domains embedded in the metastable Pu-Ga host, and its occurrence in the phase diagram would most likely be in the inaccessible negative pressure region.

B. Structural properties of σ Pu derived from x-ray PDF measurements

The local structure results from the x-ray PDF measurements and the corresponding Pu EXAFS radial distribution function (Fig. 2 lower) further elucidate beyond its *Fm*3*m* diffraction pattern how the Pu atoms of the σ structure are arranged. Although the amplitudes are somewhat affected by the experimental background and the effects of texturing, the numbers and positions of the peaks are reliable. The PDFs of the aged $Pu_{0.983}Ga_{0.017}$ and $Pu_{0.973}Ga_{0.027}$ are essentially identical in showing both the δ Pu pairs and a second set of neighbor shells in the same positions with similar relative amplitudes. What is remarkable is that this correspondence occurs despite the fact that (Fig. 2, upper) the $S(Q)$ of $Pu_{0.973}Ga_{0.027}$ displays multiple diffraction patterns that must transform into the multiple ordered structures observed in the PDF whereas, in contrast, $S(Q)$ of the $Pu_{0.983}Ga_{0.017}$ shows only the δ Pu pattern so that all of the information on the identical second structure within these data is contained within the diffuse scattering. This demonstrates that the σ

structure can occur as domains of unknown shape that are nevertheless at or below the diffraction limit in size and that are arranged aperiodically and incoherently with respect to each other within the host lattice. Over its reliable range in R, a complete curve-fit of the Pu EXAFS of $Pu_{0.973}Ga_{0.027}$ that allowed neighbor shells in addition to those of the δ structure also gives a distribution function that is identical to those of the PDFs within experimental error. The presence of the σ structure and its arrangement of atoms are thus corroborated by two completely independent measurements on these two pieces cut from the same foil.

Further evaluation of structural parameters is best done from the PDFs because of their greater data range; ordered σ neighbor atom shells occur through (and past) the 10 Å upper bound of the figure. These can be interpreted by comparison with the two calculated $g(r)$ functions that overlap at the bottom of Fig. 2. One is for fcc δ Pu that is fully represented in the PDFs. The other, more complicated one is the sum of the PDFs for δ Pu and 25% of the second, expanded fcc structure dictated by the second diffraction pattern. This combination successfully describes all of the observed features in $g(r)$ beyond 4 Å. Below 4 Å, Pu atoms are found at 3.8 Å instead of the expected 3.51 Å. However, the average 3.5 Å distance is maintained if these are balanced by another shell at 3.2–3.3 Å that then overlaps with the nearest neighbor δ shell at this same distance. In two dimensions, this split is attained by taking a 2×2 expansion of a square unit cell by and then modulating the structure by expanding one square and contracting its opposite one on the diagonal, converting the other two squares to rectangles (Fig. 3). Interstitial atoms added to the large squares then maintain the density. Analogous operations would give similar results in three dimensions. However, despite having diffraction, PDF, and EXAFS data and the success of this two-dimensional process in describing the results, we have been unsuccessful in devising a three-dimensional arrangement of the atoms that conforms to all of these results, leaving it as a challenge. This modulation, however, produces most of the experimental parameters. The minor peaks indicating this superlattice for σ would be negligibly small in the diffraction pattern that is already dominated by the δ Pu, especially if there was some aperiodic disorder in the underlying displacements. With respect to the PDF, the rapid convergence with increasing distance to a structure identical to the unmodulated one is expected because the separations between the split shells fall below the resolution limit quite rapidly with increasing distance for nonzero angles.

Some intriguing, albeit possibly coincidental, observations may relate to the origin of this modulation. First, the modulation creates atom pairs separated by close to the 3.28 Å Pu-Pu δ bond length of the δ phase, which may help accommodate the $\sigma - \delta$ interface and/or reflect aspects of the electronic structure when the f electrons are contracted and nonbonding and also its possible anisotropy [58]. In addition, the ratio of the two distances caused by the splitting of the nearest neighbor shell at 3.5 Å is that for the bcc/tetragonal (bcc/t) structure that would be generated by the classic martensitic Bain transformation applied to an $a = 5.0$ fcc lattice. Finally, the description of the σ structure as a multiplied and subsequently modulated *Fm*3*m* one with $a = 4.95$–5.00 Å is necessarily incomplete because this would result in a significant decrease of the bulk density

of the material that does not occur. There must be just enough interstitial atoms to conserve the density of δ Pu, and their most obvious location would be in the expanded components of the modulated structure (Fig. 3). In two dimensions, expanding the lattice using the actual values from these results and placing interstitials into these sections gives Pu-Pu distances within the range of the short ones in the α phase. If they are disordered so as to produce a range of Pu-Pu distances with a "glassy" distribution that is relatively constant instead of peaked, they may be invisible to EXAFS because of interference effects [41,52] and difficult to observe in PDF, especially when the number of atoms within the range is low.

C. The composition of σ Pu and the homogeneous/heterogeneous boundary

Describing additional characteristics of the σ structure, the heterogeneity, and its coupling to the concentration of δ stabilizer is accomplished via the greater quantitative accuracy of EXAFS with respect to the nearest neighbor shell and its elemental specificity. The Pu $\chi(R)\,(= \text{FT}(k^3\chi(k)))$ EXAFS of a variety of δ Pu alloys stabilized or retained with In and Ce in addition to Ga and prepared by different procedures from different Pu sources divide into two sets. Spectra in the first set deviate significantly from the calculated spectrum of δ Pu and display tremendous variability in doing so, most likely because of disorder, (Fig. 4, upper, showing ten representative spectra). Ones in the second set resemble the calculated spectrum relatively closely (Fig. 4, lower, showing six representative spectra). Materials that contain σ must fall into the former category. This dichotomy based on the appearance of their spectra gives an identical division on the basis of their compositions. Pu-Ga alloys with Ga concentrations ≤ 3.3 at. % and the Pu-In alloy whose composition is also close to the $\alpha - \delta$ phase boundary constitute the first set, whereas Pu-Ga with Ga or Ga + Am (another δ stabilizer) concentrations ≥ 3.3 at. % and the Pu-In/Ce δ alloys with In/Ce concentrations substantially greater than the phase boundary fall in the second. The structural origin of this effect was elucidated by examination of the residual difference spectra from curve-fits with the first five δ neighbor shells (Fig. 4 insets), calculated as the data minus the fit using only Pu neighbor shells that, based on their distances, correspond to those of the δ structure. These residuals reveal that, as expected, the second type of spectrum contains contributions greater than the noise level from only the neighbor shells of δ Pu whereas the first type, regardless of the shape of the original spectrum, shows a spectral feature that is the contribution of the Pu shell at 3.8 Å that belongs to the σ structure. The spectra from samples assigned to pure δ do, however, continue to display a small peak around $R = 3.9$ Å that cannot be a Fourier transform (FT) side lobe since this has been subtracted from the data and may explain why a recent report utilizing curve-fitting analysis finds σ Pu through higher Ga concentrations [25]. Even if some residual σ Pu remains in the materials, these results nevertheless demonstrate a dramatic change in its occurrence around the 3.3 at. % Ga level. The remaining variability in the spectra reflects disorder that can result from the processing but also from differing impurity types and amounts that can have, for example, significant effects on the phase stability
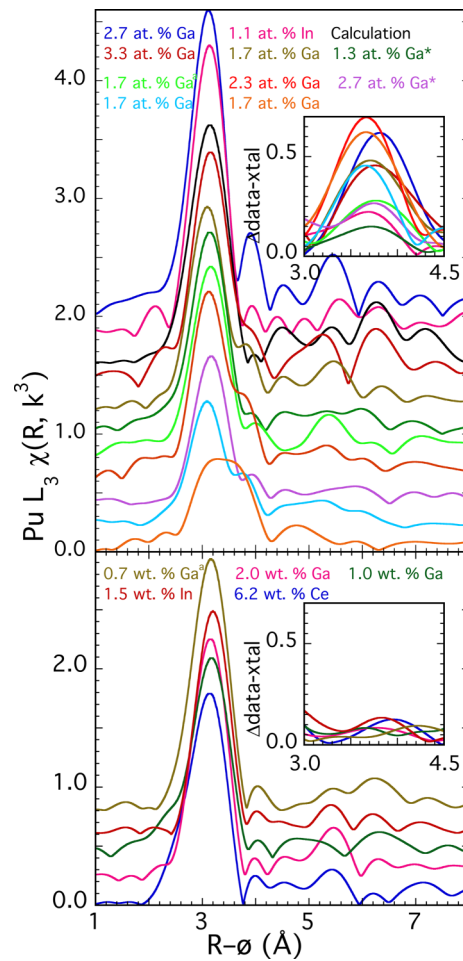

FIG. 4. (Color online) Fourier transform moduli calculated from the Pu L_3 EXAFS spectra $[\chi(R, k^3) = \text{FT}(k, k^3\chi)$ for $k = 5.4$–12.8 Å^{-1} using 1.0 Å^{-1} wide Gaussian windows] of a diverse set of δ Pu alloy samples (* = the samples containing negligible amounts of Pb and Sn as described in the experimental section, ^{a} = aged). The spectra from top to bottom correspond to the labels read from left to right (color in online version). Spectra measured at 80 K will have larger thermal Debye-Waller factors and lower amplitudes relative to those measured at 25–40 K. The upper figure contains the spectra of new PuGa/In materials with lower concentrations of δ stabilizer that display considerable variability consistent with disorder that includes a significant contribution from the σ Pu shell at 3.8 Å. The lower figure contains the spectra from PuGa/In/Ce/Ga-Am alloys with higher concentrations of the δ stabilizing element(s) that are much more similar to each other and to the calculated spectrum of fcc δ Pu in the upper plot. The residual difference spectra of the upper samples obtained after subtracting a curve-fit with only the first five neighbor shells of the δ structure (inset), despite the wide variability in the appearance of the original data, all consistently display a prominent feature near 3.7 Å that is subsequently well fit by the Pu shell at 3.8 Å that is part of the σ structure. The data for the lower set of samples are well fit with just the δ neighbor shells so that their difference spectra exhibit only relatively modest residuals whose real components (not shown) do not match those above. Note that only half of the χ information is shown in the FT modulus. The real/imaginary component, which has been omitted for clarity, provides a definitive means for separating overlapping contributions and determining which modulus features originate in simple Pu shells or are merely side lobes or other artifacts.
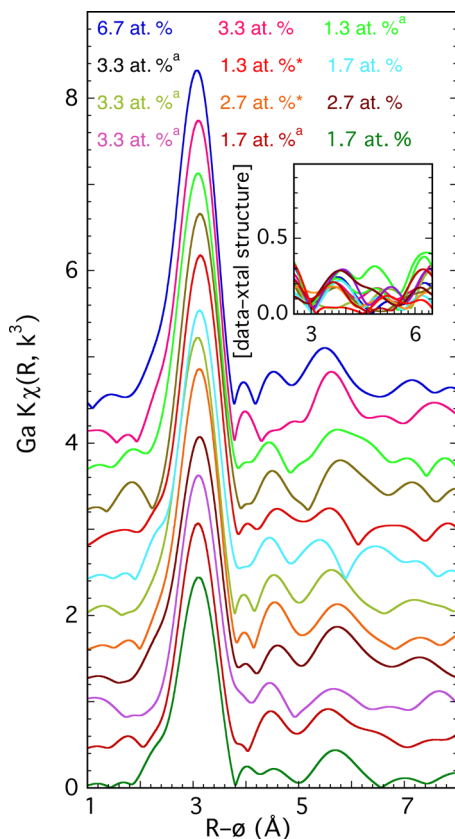
FIG. 5. (Color online) The Ga K edge EXAFS of many of the same samples as in Fig. 4, shown as FT moduli [$\chi(R, k^3) = \mathrm{FT}(k, k^3\chi)$] for $k = 5.3$–12.0 Å^{-1} also with Gaussian windows]. Reading the labels from left to right corresponds to the spectra from top to bottom (* = the samples containing negligible amounts of Pb and Sn as described in the experimental section, ^{a} = aged). In contrast to their Pu counterparts in Fig. 4, these spectra are all very similar to each other, indicative of a corresponding similarity in the highly ordered Ga environments. Subtraction from the data of the first three shells of a quasi-fcc structure in which the proximal Pu atoms are contracted around the smaller Ga with the contraction diminishing with increasing Ga-Pu distance reveals (inset) that this model of the structure is largely complete and that there is, in contrast to the Pu, no dependence of the local structure on the Ga concentration.

[31]. Therefore, these results demonstrate that: (1) Pu-Ga (and comparable In) alloys on the low side of 3.3 at. % Ga are heterogeneous $\delta - \sigma$ where the δ host may exhibit substantial disorder; (2) Pu-Ga and comparable In and Ce alloys on the high side of this concentration are homogeneous δ that tends to be well ordered; and (3) that the region of overlap, because of differing impurity levels and preparation methods, is small.

The Ga K edge $\chi(R)$ (Fig. 5, containing twelve representative) spectra from these same samples all show three prominent features through $R = 6$ Å that are independent of composition [20,21,25,35,36,59,60]. Curve-fits demonstrate that these features correspond to the first three shells of a contracted, quasi-fcc cluster that is nevertheless highly ordered with respect to the widths of these shells and that (Fig. 5, inset) this fit accounts for most of the spectral weight to the noise level with no trends with composition. The nearest neighbor Ga-Pu distance is 0.11–0.13 Å shorter than the Pu-Pu

[21,25,32–36]. This contraction decreases with distance so that by the third shell $\Delta(R_{\mathrm{Pu\text{-}Pu}} - R_{\mathrm{Pu\text{-}Ga}})$ it is only 0–0.02 Å, significantly less than the 0.045 Å expected by extrapolating the nearest neighbor distance with Vegard's law, and the strain field around the Ga has relaxed. The Ga neighbors are more thermally and statically ordered than those around the Pu [35–37]. Thus, although the Ga is substitutional and expanded relative to its expected size, it nevertheless compels the Pu to conform to its preferred structure rather than vice versa.

The significance of these results for the Ga is that they differ from the Pu by displaying only the quasi-fcc type of spectrum across the entire range of composition whereas the Pu is heterogeneous at lower Ga concentrations. Since the Ga never exhibits any indication of a second type of structure even when the material as a whole is heterogeneous $\delta - \sigma$, it must reside exclusively in the form that is retained and homogeneous at higher Ga concentrations, i.e., the δ host. The σ domains therefore cannot include the Ga atoms so that σ Pu forms in regions that are locally depleted in Ga. This is consistent with Ga promoting the formation and retention of δ Pu, not only phenomenologically in bulk material, but also microscopically on the angstrom to nanometer scale in proximity to the individual Ga atoms.

D. Comparison of calculated and experimental EXAFS spectra

Additional identification and characterization of lattice distortions, such as the Pu shell at 3.8 Å that is the signature of the of σ structure, will be performed using the data from the set of identically prepared alloys made with the zone-refined Pu [45] that have lower noise, greater range, and were all measured at lower temperature (35 K). A starting point is to compare the experimentally measured $\chi(R)$ (=FT ($k^2\chi(k)$)) EXAFS representation with those calculated from the crystal structure by one of the highly accurate codes written for this purpose, such as FEFF [53]. Especially significant is if and how the EXAFS, and by implication the local environments, of the various elements differ from those of Pu and each other.

The EXAFS calculated from the crystal structure of δ Pu resembles its pair distribution function $g(r)$ with a well-resolved peak for each shell of neighbor atoms through the fifth (Fig. 6). This is because, in the fcc structure with a large lattice constant, the neighbor shells do not overlap with each other, and the multiple scattering contributions are sufficiently broad and low in amplitude so that they do not perturb this correspondence between $\chi(R)$ and $g(r)$. The experimental data, however, do not behave the same way. In contrast to, for example, Cu that is known not to possess any disorder, in addition to the relative amplitude reduction beyond the nearest neighbor shell resulting from the distance dependence of the Debye-Waller factor, the measured EXAFS of Pu exhibits additional modulus peaks of various sizes and shifts in the real components of the spectra on the sides of and in the flat regions between the primary δ ones found in the calculation [34]. The ones that overlap with the nearest neighbor peak at $R = 3.2$ Å will be discussed in detail below, and beyond the large contribution of the third shell with its 24 atoms, the inverse square distance dependence of the amplitude and the increased Debye-Waller factors significantly diminish the amplitudes and increase the susceptibility to noise even in high
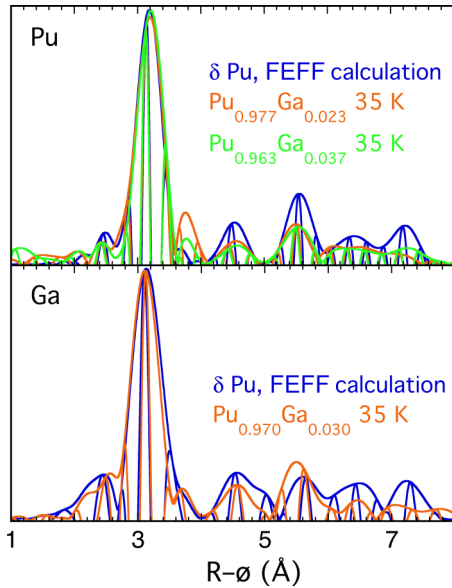
FIG. 6. (Color online) Calculated and experimental Pu and Ga $\chi(R, k^2)$ [= FT($k, k^2\chi$) for $k = 3.7$–15.75 Å^{-1} for Pu and 3.0–13.5 Å^{-1} for Ga with sine windows] spectra using the δ Pu crystal structure for Pu and the local contraction determined from the EXAFS for Ga. Transform moduli and real components are shown.

quality spectra. The spectra from $R = 3.6$–6.0 Å are, however, both credible and informative. The peak near $R = 5.6$ Å that is the third neighbor shell contribution is uniformly large and consistent in all of the Pu spectra except at the highest Ga concentrations, duplicating its behavior in the calculation. In contrast, the contribution of the second shell is complicated. Its modulus is shifted higher than the calculation and real component lower, indicative of a difference that over other data ranges causes the amplitude to spread over shoulders and other peaks around it that differ among the various samples. Although curve-fits that include only a single Pu shell in this region do find one, the numbers of atoms are small, the errors in the distance are large, and the correspondence between fit and data is poor, indicating that the six atoms of the second neighbor shell around the Pu are split. Good fits actually require two or three shells between 4.4 and 4.9 Å (σ Pu has a neighbor near 5 Å). There is one three-leg scattering path 0.3 Å longer than the second neighbor shell that might contribute to this complicated behavior, but insofar as it is much smaller than the actual second shell contribution and would be rapidly reduced by disorder, it is unlikely that its effect would be significant.

The Ga-Pu bond length is around 0.12 Å shorter than the Pu-Pu one, with this contraction relaxing to 0–0.03 Å by the third neighbor shell. Propagating this contraction apparently separates the second shell contribution from the overlapping, altered multiple scattering one from the triangular paths involving the first shell Pu atoms so that the calculated Ga $\chi(R)$ shows a large shoulder on the high R side of this second shell peak (in Fig. 6 at ~5 Å, blue curve in online version). In addition, the relative amplitude of the third shell peak is reduced to close to that for the second shell. This latter characteristic is duplicated in the experimental spectra, but not the calculation, so that the Ga spectra differ from the Pu $\chi(R)$ by displaying three large,
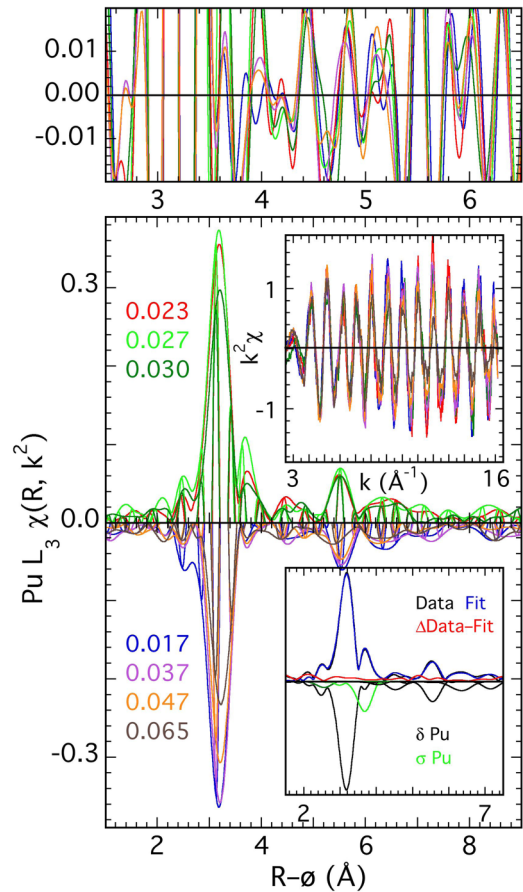

FIG. 7. (Color online) Pu EXAFS spectra $\chi(R, k^2)$ for $k = 3.7$–15.85 Å^{-1} (moduli and real components, sine windows) from δ Pu-Ga samples made from zone-refined Pu and the Pu$_{0.973}$Ga$_{0.027}$ sample made from electrorefined Pu whose diffraction pattern and PDF are shown in Figs. 1 and 2. The numbers are the atomic percent Ga. The upper plot shows only the real component so that the nodes can be compared to show regions where the spectra, and by implication the structure, are identical—$R = 2.9$–3.5, 4.3–4.5, 4.8–5.0, and 5.4–5.8 Å^{-1}—and where they differ as a function of composition. The lower plot shows the spectra of samples containing the σ structure in the upper half and spectra of samples not possessing the σ structure in the lower. As described in the text, the spectrum of Pu$_{0.935}$Ga$_{0.065}$ departs from the others at 35 K but more closely resembles them at 90 K. The upper inset shows $k^2\chi(k)$; the direct overlay shows how they differ principally in the Debye-Waller factor. The lower inset shows the FT moduli of the data, fit, and difference for the Pu$_{0.973}$Ga$_{0.027}$ sample, and (inverted) the moduli of the individual contributions of shells of neighbor atoms making up the fit, allowing the features in $\chi(R)$ to be assigned to these structural components. Contributions from shells of atoms that are not part of the δ crystal structure are in green in the online version, whereas δ components are black.

well-separated, symmetric peaks (and a small one on the high R side of the nearest neighbor peak) that can putatively be assigned to the first three neighbor shells. Multiple scattering contributions also appear negligible despite the indications in the calculation, at least in part because the calculation exaggerates them by applying the same Debye-Waller factor to all paths. Because of the high quality of the available Pu-Ga spectra (see Figs. 6–8), it is worth extending these
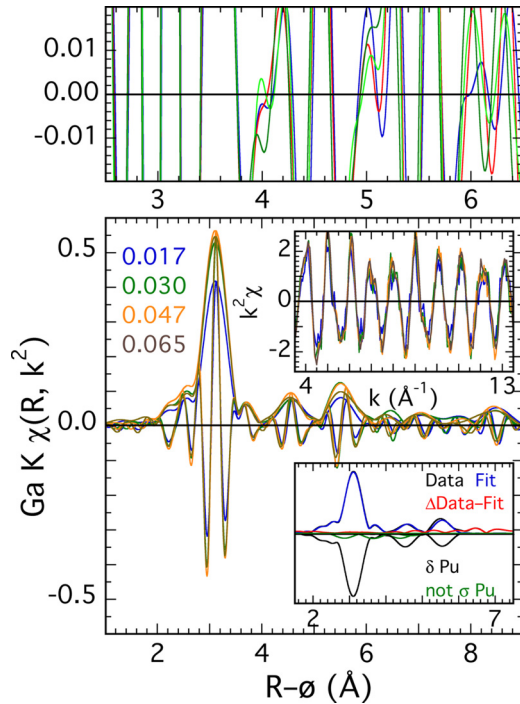
FIG. 8. (Color online) Ga EXAFS spectra [$\chi(R,k^2)$], moduli and real components of the FT of the k^2-weighted $\chi(k)$ data from $k = 3.5$–13.5 Å^{-1} with sine windows, from the same set of δ Pu-Ga samples as in Fig. 6. The numbers are the atomic percent Ga. This figure is the same as Fig. 7, with the upper part expanded to show the nodes of the real components, the lower with the full spectra, and the top inset being $k^2\chi(k)$. The lower inset showing the fit components is of Pu$_{0.970}$Ga$_{0.030}$ as used (Fig. 10) to identify non-δ components including the fourth and fifth shell contributions that were near their correct distances but with greatly reduced amplitudes that gave relatively large errors because of their small size in these spectra.

comparisons to the fourth and fifth shells. These are lower than the third shell contribution in the Pu $\chi(R)$, matching their behavior in the experiments. However, because of the reduced third shell amplitude in the calculated Ga $\chi(R)$, the more distant contributions remain as large as it is. This pattern is not observed in the measured Ga $\chi(R)$, where the fourth and fifth shell contributions are small and the fourth shell one varies substantially between the different samples. Therefore, although there are aspects of the resulting spectra that match the calculation, there are others in which it does not [61], and there are several ways in addition to the contraction in which it fails to duplicate the Pu. The Ga site may therefore not be purely substitutional in the sense that the only lattice distortion it causes is the contraction and is otherwise identical to the Pu.

E. Trends in the local structure with Ga concentration and the organization of the Ga into a quasi-intermetallic

In Fig. 7, the Pu $\chi(R)$ EXAFS spectra at 35 K are shown for the set of identically prepared δ Pu-Ga samples made from the zone-refined Pu spanning 1.7–6.5 at. % Ga and the Pu$_{0.973}$Ga$_{0.027}$ sample homogenized for a longer time made from electrorefined Pu. The δ components of the

structure are easily located by curve-fits in all of the spectra, although the errors for the more distant shells become large as the materials become less ordered and the anharmonicity in the distributions affects the fits (Table I). As the Ga concentration increases, the local order, which is coupled to the amplitude of the modulus peaks, decreases, which is expected as more atoms are shifted from their lattice sites due to contraction of the structure around the smaller Ga atoms. The more extensive homogenization of the Pu$_{0.973}$Ga$_{0.027}$ sample may explain why its spectrum displays the highest amplitudes of all. At 6.5 at. % Ga, the disorder is so extreme that, not only is the amplitude of the nearest neighbor contribution significantly reduced, but also features assigned to the more distant shells deviate substantially from the other spectra. (Similar behavior is displayed by the Pu$_{0.953}$Ga$_{0.047}$ spectrum at 90 K in Refs. [21,37], consistent with the equivalence of composition and temperature in martensitic materials [62,63].) This trend, however, is interrupted between 3.0 and 3.7 at. % Ga, where the amplitude of the nearest neighbor peak gets larger prior to resuming its monotonic decrease [37]. This unexpected occurrence is accompanied by the loss of the feature near $R = 3.7$ Å that is the contribution of the 3.8 Å Pu neighbor shell of σ Pu. The loss of the σ structure in these samples therefore occurs at exactly the same Ga concentration as was found for the other wide variety of materials. This sample of Pu$_{0.983}$Ga$_{0.017}$ is exceptional in not showing the σ Pu peak in its spectrum, the only material of this composition not to do so. It does, however, display somewhat higher spectral amplitude on the low R side of the nearest neighbor δ peak.

These higher quality spectra convincingly demonstrate what could only be inferred before, that, with the exception of the Pu of the sample with the lowest Ga concentration where the pattern of the peaks is identical although the amplitude is somewhat lower, the Ga environments (Fig. 8) do not display the expected diminution of amplitude with increasing amounts of Ga but are identical within the noise level [25,34]. This result is not just an oddity, it is profound in its implications for the arrangement of the Ga atoms in δ Pu. Molecular dynamics-type modeling, in which the atom positions are relaxed for a given set of relative potentials for the different atom pairs [42–44] using the measured Ga/Pu-Pu distances in which the relative bond strengths of the various Ga/Pu-Pu bonds are varied, shows that this effect cannot be duplicated in structures when the Ga atoms are randomly distributed throughout the lattice until the Ga-Pu bond strengths are many hundreds of times as great as the Pu-Pu ones. In this modeling, as the Ga concentration increases the peaks in the Ga partial $g(r)$ always become much broader, especially at higher R, so that this behavior of the spectra cannot be achieved in any physically realistic scenario. Ga concentration-independence of $g(r)$ is, however, automatically attained if the Ga positions are semiordered so that there is a long Ga-Ga distance that is more highly probable around which neighboring Ga atoms form a Gaussian. The result is a quasi-intermetallic, where the larger separations between the Ga atoms and lower interaction energies between the Ga sites result in preferred rather than precise positions that are better described as an increased probability that is still less than unity for a given site [64]. One characteristic of this phenomenon is that it is applicable to any Pu:Ga ratio, not just those few where a periodic unit

cell can be formed. A corollary to this type of distribution would be that, if these probabilities are different in different directions, small tetragonal or orthorhombic distortions will occur [23,65]. We have shown that, if differently oriented domains of chemically ordered structures are coherent at their interfaces, then the expected splitting of the diffraction peaks will not occur because the strain is distributed over all of the atoms, and the distortion is averaged out over the entire crystal [43,44]. Breaking this registry at the interfaces, such as might occur during the initiation of the martensitic transformation or from radiation damage, allows the domains to relax and exhibit their lower symmetries while concomitly stabilizing the dislocations or other types of defects [43].

Based on the ~3.3 at. % Ga concentration where the σ structure ceases to be observed under the assumption that δ Pu first saturates the crystal, the expected composition of this quasi-intermetallic would be around $Pu_{25-35}Ga$ (or $Pu_{0.968}Ga_{0.032}$). In terms of bulk properties, this is the same as the boundary between stability vs metastability with respect to the martensitic transformation. Furthermore, this limit is "coincidentally" arrived at in yet a third way. Insofar as the measured contraction at the third neighbor shell is at the error limit of the method for zero, it would be reasonable to assign a diameter of around 11–12 Å to the extent of the strain field around a Ga atom. If the Ga atoms are distributed evenly throughout the crystal, then $Pu_{30}Ga$ is close to where the boundaries of these local strain fields all come into contact with each other, filling the crystal. It is of obvious interest to check if the existence of a stable $Pu_{30}Ga$ phase would resolve any of the ambiguities in the phase diagram, e.g., the stability of $Pu_3Ga + \alpha$ Pu relative to δ Pu-Ga as a random solid solution, or whether it is simply a somewhat lower energy form or different admixture of quantum states [14,15] of a metastable material. Admittedly it is a radical proposal, but the arrangement of atoms below the diffraction limit that is the objective of local structure measurements often is. It is, however, only contradictory to more conventional crystallographic models when the complementarity of local and long-range average structure is neglected.

The preferred organization of the Ga atoms into $Pu_{25-35}Ga$ also assists in explaining the formation of σ Pu. The formation of a second structure resulting from a fluctuation in the local (nanoscale) composition below the $\alpha - \delta$ phase boundary requires a volume large enough so that the phase stability energy is greater than the epitaxial strain at the interface between the two structures, which could be expected to be several dozen or even the few hundred atoms that define the diffraction limit. This aggregation of the Ga promotes the formation of these relatively large domains that are depleted or devoid of Ga.

F. Identification of additional δ lattice distortions via residual spectra

Corroboration for this model for σ and other types of individual or collective lattice distortions and heterogeneity is perhaps best obtained from inspections of the residual or difference spectra after a curve-fit to the EXAFS containing only the crystallographic δ shells is subtracted from the data [37]. The level of detail explicit in this method is consistent with the excellent signal:noise levels in the spectra from this
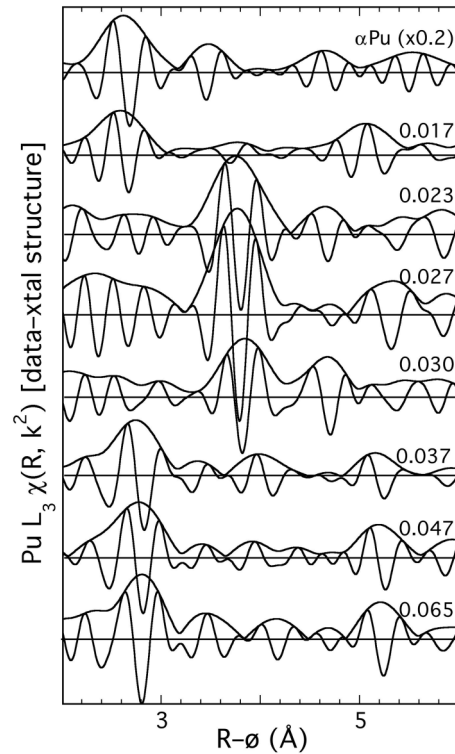

FIG. 9. Residual Pu spectra of the Fig. 7 samples with numbers indicating the atomic percent Ga obtained by subtracting the curve-fit including only the first five shells of the δ structure (optimized by allowing R, N, and the Debye-Waller factor to float for each shell) from the data. Spectral features that are either large relative to nearby ones assigned to neighbor atom shells or that show consistent patterns correlated with composition are indicative of non-δ aspects of the structure. A spectrum of α Pu reduced to 20% of its actual amplitude is included for comparison with the residual from the $Pu_{0.983}Ga_{0.017}$ sample.

final suite of samples. Smaller residual features found in only one spectrum—mostly at low R below the contributions from structural features—are noise, while those observed in the spectra from all compositions most likely originate in unfit multiple scattering features from paths involving the major neighbor shells or artifacts resulting from differences between the actual and calculated phases and amplitudes. However, features that track the composition or other extrinsic variables or that are large relative to those assigned to structural components most likely represent shells of atoms in local lattice distortions adventitious to the δ crystal structure. In addition, the behavior of the real component of the transformed spectrum $\chi(R)$ relative to the modulus can indicate whether the spectroscopic feature originates in a well-ordered single site Gaussian type of Pu shell or a multiple site anharmonic distribution of atoms. In Pu EXAFS transformed over this data range, the former are associated with a spectroscopic feature where the modulus maximum coincides with a minimum in the real component.

The σ shell with a Pu-Pu distance near 3.8 Å that was already shown for all of the samples in the upper half of Fig. 3 is easily observed in these residuals from this complete, highest quality sample suite (Fig. 9) as the feature close to $R = 3.8$ Å that occurs only in the spectra of the samples with

2–3.5 at. % Ga. That it is completely absent from the other spectra demonstrates that it is not an artifact of the measurement or analysis that is simply more prominent in these spectra. This procedure therefore corroborates the interpretation derived from inspection of the full spectra and the curve-fit results. It also illuminates additional spectroscopic features of varying significance that suggest further complexity in the σ and $Pu_{30}Ga$ structures. For example, the $R = 3.8$ Å modulus peak is immediately followed by a kink in the real component (cf. the PDFs) and another, smaller (very small for $Pu_{0.973}Ga_{0.027}$) Pu-shell-like feature at $R = 4.6$ Å that overlaps with but is separate from the second nearest neighbor δ shell. Of greater import are the features near $R = 5.2$ Å for the samples with Ga concentration >3.5 at. % (and possibly the more homogenized $Pu_{0.973}Ga_{0.027}$) and the even larger one at $R = 2.8$ Å that is indicative of a Pu shell near this distance that is almost 0.5 Å shorter than the δ nearest neighbor. Since these samples are oversaturated with Ga relative to the $Pu_{30}Ga$ stoichiometry of the δ quasi-intermetallic, this feature could reflect distortions resulting from the forced incorporation of excess Ga into the $Pu_{30}Ga$ structure, exacerbated if the Pu-Pu bonding is anisotropic [58]. However, since this should result in a correlation between its magnitude and the Ga excess, an alternative explanation is that $Pu_{30}Ga$ itself may accommodate the Ga-induced strain via additional localized but ordered displacements of Pu atoms that produce some highly contracted bonds. For now, the question remains of whether this is part of $Pu_{30}Ga$ or a response of its structure to the incorporation of additional Ga inhomogeneities that maintain their local environments. Since the cubic diffraction pattern is not perturbed, these short Pu-Pu pairs must be aperiodically distributed. These residual spectra also demonstrate the caution required in interpreting low frequency, nonreproducible aspects of spectra; the additional complexity of the $\delta + \sigma$ mixture apparently increases the difficulty of approximating the smooth background with the spline polynomial so that these spectra all exhibit variable patterns of significant magnitude below $R = 3$ Å despite the high degree of similarity in their original spectra.

This same procedure has also been applied to the Ga spectra (Fig. 10), with one difference being that a simple, single site Pu shell neighboring Ga has the maximum of the real component at the modulus peak. Since the only effect of composition on these was the diminished amplitude from the $Pu_{0.983}Ga_{0.017}$ sample, even with the enhanced sensitivity to changes in the spectra afforded by this method, only minimal differences between the spectra are expected. This is what is observed. The fit with the crystal structure as the basis does, however, leave a large number of residuals that are very similar in all of the spectra and that were mostly fit with relatively small non-δ type Pu shells (Fig. 8, lower inset), consistent with the deviations of the experimental from the calculated spectra (Fig. 6). The largest of these, at $R = 3.6$ Å, directly overlaps with but is small relative to the first nearest neighbor contribution, and its pattern does not match that of a simple Pu shell. It is therefore quite possibly an artifact from an error in the calculation of the Ga-Pu amplitude and phase. However, comparison with the calculated spectrum indicates that the double peak at $R = 4.8$–5.3 Å (low in the spectrum of $Pu_{0.983}Ga_{0.017}$) and the features at and beyond $R = 6.8$ Å are contributions from non-δ shells of atoms.
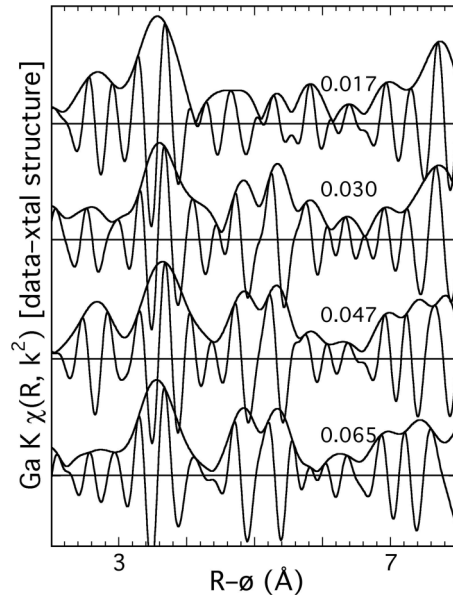

FIG. 10. Ga residual spectra calculated as in Fig. 9.

As with the Pu, these point to specific, Ga-centered distortions of the $Pu_{30}Ga$ structure from cubic [61]. The spectral features these Ga residuals display are, however, not the σ, (*vide infra*) σ', or δ ones observed for Pu but are specific to the Ga. In fact, although the predominant characteristic of the Ga is its substitution for the Pu directly into a contracted cubic site, a comparison of the Pu and Ga total $\chi(R)$ shows some distinct differences that complicate this picture, as discussed above vis-à-vis the comparisons with calculated spectra and the curve-fit results. It is difficult to explain, for example, the relatively large amplitude of the second shell since the greater disorder around the Pu would suppress multiple scattering resonances that would interfere with its contribution so the net result would be to enhance the amplitude. The most likely explanation is that lattice distortions and deviations of $Pu_{30}Ga$ from a simple cubic structure, such as those observed in the residual spectra, involve a sufficiently large fraction of the atoms that their contributions—or lack thereof if they are disordered—exert a correspondingly large and uneven effect on the amplitudes of the spectra.

G. The σ' structure

Although only a single sample contains the σ' structure, its virtual identity with the EXAFS from the complicated nearest neighbor distribution in and its origin in Ga-depleted domains that would transform to the α phase if not embedded in the δ host call for its evaluation. As described above, in order for the σ structure to contain the same number of atoms per unit volume as δ Pu, it must contain aperiodically disordered interstitials that, when placed within its more open parts, give short α Pu-like Pu-Pu distances. Insofar as α/α' Pu is the stable bulk phase for Pu containing less than around 1.0 at. % of Ga at ambient and lower temperatures, an α-like structure might be expected. Nondiffracting domains of a second structure that form during cooling have been inferred from a symmetry lowering broadening of the δ Bragg peaks. These were labeled α' nucleation sites or embryos [29], but this contradicts the fact

that they formed without changes in the overall volume of the crystal [23]. Then again, embedded, Ga-depleted nanodomains of α-Pu that formed by transformation during cooling would be under considerable tension exerted by the δ host lattice and therefore could be considered as under substantial negative pressure. This type of microscopic tension effects transitions to otherwise inaccessible phases in, for example, Fe [66–69]. In fact, α Pu strained to failure by uniaxial tension has been found to fracture by a ductile mechanism [5], demonstrating that negative pressure does foster δ or some other high symmetry structure. We have identified σ Pu as a lower density form of Pu in addition to those found in the phase diagram whose structure is modulated to preserve Pu-Pu bonds identical to those in the δ phase. Nevertheless, it would be in some sense satisfying to find some of the structural attributes of α Pu in the σ structure since it also could be considered as forming in anticipation of the $\delta \rightarrow \alpha$ transformation as the finest scale/broadest temperature range "texture" that is a characteristic of martensites in the fluctuation region in proximity to their transformation [30,62,70–79].

A tendency for such Pu clusters with little to no Ga to form α/α' Pu would explain the anomalous behavior of this particular $Pu_{0.983}Ga_{0.017}$ sample. Insofar as it was prepared from ultrapure Pu stock while the other, less pure samples with identical nominal composition but with more impurities uniformly showed $\delta-\sigma$ heterogeneity, once δ is stabilized inhomogeneities may emulate Ga in their effects on the nanostructure. What would then be unique about this sample is that, at this lowest (effective) Ga concentration, the Ga-depleted domains that form after the Ga has organized into $Pu_{30}Ga$ would be larger in size than at higher Ga concentrations or at the same one but with higher impurity levels. Large domains would enhance the contribution of the phase stability in the formation of their structure while reducing that of $\delta-\sigma$ interfaces and would therefore tend to reinforce aspects of the α structure. If the σ structure did possess sets of both short, α-like bonds and longer, δ-like bonds, larger domains could be expected to promote ordering around the former and smaller domains around the latter. The average structure in terms of the generalized positions of the atoms relative to each other could therefore be conserved even as the local ordering is modified by displacements from these positions. We have named this alternative local arrangement of atoms "σ'."

This still leaves unanswered the question of why the amplitude of the Ga EXAFS was reduced for this sample. In addition to the local ordering, a second difference between σ and σ' that is also consistent with larger domain sizes is the significance of its geometrical relationship with the δ host. For $Pu_{0.983}Ga_{0.017}$, the absence of the σ feature is balanced by a shifting of spectral weight in $\chi(R)$ to the shoulder at $R = 2.5$ Å, as would be expected if the order of a set of short Pu-Pu bonds is enhanced at the expense of a set of longer ones. In the Ga spectra of this sample, there are no corresponding counterbalanced changes in amplitude, only a diminution that does not occur when the σ feature is either present or absent in the Pu spectra of all the samples with higher Ga concentrations. So although all of the Ga for samples with greater than 1.7 at. % Ga is in the $Pu_{30}Ga$ part of the material, some fraction of the Ga atoms are not in the $Pu_{30}Ga$ component of $Pu_{0.983}Ga_{0.017}$

but must instead be within a locally disordered environment in the non-$Pu_{30}Ga$ domains, i.e., the σ' regions. The smaller σ domains present at higher Ga concentrations are therefore destabilized relative to δ by even small amounts of Ga so that the exclusion of the Ga from σ Pu is more rigorous. In contrast, the larger σ' ones are more intrinsically stable and less finely balanced against disruption by the incorporation of inhomogeneities. On the micron scale, the geometry of α' Pu inclusions is fixed so as to minimize the strain energy with respect to the δ host, and the observation of such inclusions cutting across Ga-enriched grain centers indicates that the incorporation of Ga into the α structure is just one contribution and not the dominant one to the total energy [5,27,30]. Their geometry within the host is therefore determined more by the arrangement of atoms at the interfaces between the structures and the accommodation of the stress via the elastic tensors so that, although σ' forms preferentially in Ga-depleted regions, it will nevertheless develop in a way that includes some Ga atoms that will distort and disorder their environments to eliminate short Ga-Pu bonds [28].

Finally, in terms of the $Pu_{0.983}Ga_{0.017}$ sample exhibiting α-like tendencies as in the full spectrum, no trace of a feature near $R = 3.8$ Å is observed in its Pu residual (Fig. 9). Instead, at around $R = 2.6$ Å is a feature whose real component shows that it is not a single Pu shell. Comparison with the spectrum of α Pu demonstrates, remarkably, that it is identical to the complicated spectral contribution from the milieu of short distances in α Pu [80], but reduced to around one-fifth the amplitude. The range of Pu-Pu distances and anharmonic nature of the distributions that occur in monoclinic α Pu in contrast to the strictly single site ones in cubic δ and quasicubic σ explain why the σ spectral feature in the full spectrum is so high in amplitude and gives such a clear signature whereas the effect of σ' is the more subtle enhancement of mean peak's shoulder at $R = 2.5$ Å. For equivalent numbers of atoms, the narrow σ contribution is prominent in both PDF and EXAFS in contrast to the broadened, low amplitude one from σ'. Since extensive diffraction analysis did not show any trace of the α Pu pattern nor are the other EXAFS components of α Pu observed, then even nanodomains of α Pu cannot be the explanation for this feature in the $Pu_{0.983}Ga_{0.017}$ residual. Instead it confirms the suggestion that there is a set of shorter Pu-Pu bonds in this material that duplicate those found in α and that do not occur at least in the same form as this in samples that contain the σ structure or that are saturated with $Pu_{30}Ga$.

Unlike the Pu residual of $Pu_{0.983}Ga_{0.017}$, the Ga one only gives a negative result in that it is missing one of the features found for all of the others. The most likely explanation is that described previously, that although the σ domains must exclude essentially all Ga, there is a cohort of locally disordered Ga atoms in σ' that do not contribute to the total spectrum so that its magnitude is diminished. The contribution to the EXAFS of a semiordered neighbor shell at around 5 Å in this σ' population overlaps with that of the $Pu_{30}Ga$ so that their EXAFS waves interfere destructively. The remainder of the Ga environment is too disordered to have any effect on the $Pu_{30}Ga$ EXAFS so the residual spectrum from this sample matches the others throughout the remainder of its range.

H. Direct approach to changes in local structure: Phase subtraction and amplitude ratioing

An important attribute of the dependence of the structure on composition is whether or not there are changes in the bond lengths. This is especially true in the interpretation of these results because it depends highly on the conservation of specific structural parameters. Accurate characterization of the composition dependence of the speciation is also required for addressing one of the basic issues in solid solutions, the relationship of the local structure to Vegard's law type behavior (since Vegard's law strictly applies only to solid solutions that extend from 0 to 100% substitution, we qualify δ Pu-Ga with "type"). Local structure data provide the opportunity to determine if the volume change follows the simple Vegard's model by giving the distances to succeeding neighbor shells [81]. Departures from Vegard's law are also of interest because they suggest that element-specific interactions are occurring.

Crystallographic departures of δ Pu-Ga from Vegard's law are well documented, with the lattice constant decreasing with a greater slope than the line connecting δ Pu and Pu_3Ga. Reported values are not always in complete agreement [19,33], but then some margin must be allowed for differing impurities and sample processing. In regards to the $\delta-\sigma$ heterogeneity, at least some results may show small discontinuities in the lattice constant, including an increase at around 3.3 at. % Ga [23,33,54], although these are not much larger than the error. Beyond the crystallography there have been conflicting reports on the dependence of the bond lengths in Pu-Ga on the Ga concentration, all based on EXAFS curve-fitting to the δ structure [25,32–34]. A direct, i.e., not involving curve-fitting, approach to extracting this information from the spectra is phase subtraction and amplitude ratioing. The former identifies differences in the absorber-neighbor distances of selected shells of neighbor atoms relative to a standard, and the latter changes in the numbers of atoms and the Debye-Waller factors. In both cases, deviations from the known functional forms of the results not only give real errors in these results instead of estimates from propagation through the multitudinous steps of the analysis but also can give indications of more fundamental differences between the sample and standard than the simple metrical parameters.

The standard selected as the basis for these analyses is the one with the lowest Ga concentration that is homogeneous δ (no σ or σ'), $Pu_{0.963}Ga_{0.037}$ for Pu and $Pu_{0.953}Ga_{0.047}$ for Ga. The analysis of the change in Pu-nearest neighbor Pu distance in these data by phase subtraction (Fig. 11, center) gives differences relative to this standard of 0.006 ± 0.002, -0.001 ± 0, -0.010 ± 0.002, 0 ± 0, and -0.005 ± 0.005 Å for, respectively, $Pu_{0.983}Ga_{0.017}$, $Pu_{0.977}Ga_{0.023}$, $Pu_{0.970}Ga_{0.030}$, $Pu_{0.953}Ga_{0.047}$, and $Pu_{0.935}Ga_{0.065}$. They therefore show no significant deviation of the distances from each other since the greatest difference is only -0.010 Å. Although some of the changes are greater than the error, there is no trend with composition through the 6.5 at. % Ga sample so that it is likely that these small differences simply reflect disorder. What is observed in the spectra from the samples with the higher Ga concentrations is a different effect, an increase in the deviation of the phase difference from the horizontal line expected of it. This suggests a departure of the phase shift for this Pu-Pu
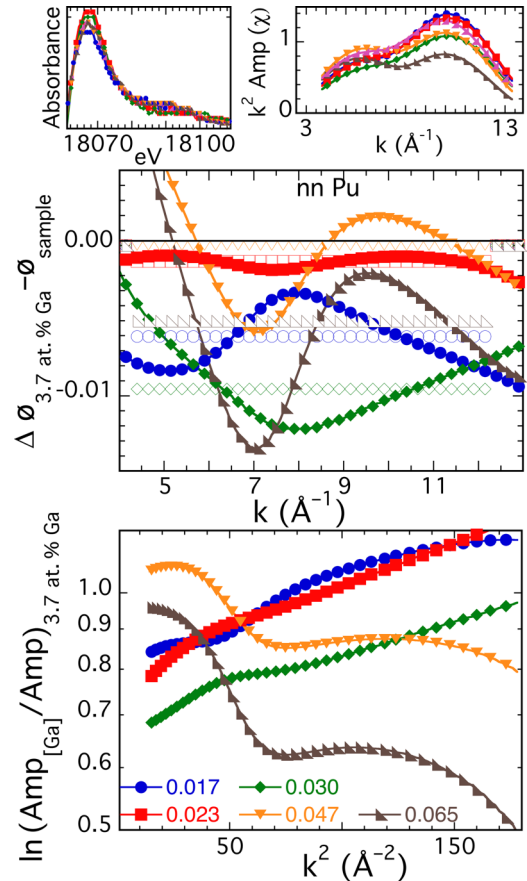

FIG. 11. (Color online) (Center) Phase differences of nearest neighbor δ Pu-Pu wave between spectra of indicated Pu-Ga samples (blue circles are for $Pu_{0.983}Ga_{0.017}$, red squares are for $Pu_{0.977}Ga_{0.023}$, green diamonds are for $Pu_{0.970}Ga_{0.030}$, orange downward-pointing triangles are for $Pu_{0.953}Ga_{0.047}$, brown left-facing triangles are for $Pu_{0.935}Ga_{0.065}$, and purple right-facing triangles in the upper two plots are for the $Pu_{0.963}Ga_{0.037}$ standard) and that of the $Pu_{0.963}Ga_{0.037}$ used as a standard (solid symbols) and the fits to the expected horizontal lines (open symbols) that are the basis for the listed results. Calculations utilize 35 K spectra. The small upper right figure shows the absorption spectra over the white line of the edge region. Insofar as the total spectra exhibit real differences from each other, the deviations from the horizontal lines expected for the phase differences are most likely real and not artifacts of the analysis. (Lower) Logarithmic plot of amplitude ratio for the same spectral components; the listed results are from a linear fit to the ln-ratio where the intercept gives the relative number of atoms in this shell and the slope gives the change in the Debye-Waller factor. The small upper left figure contains the amplitude envelopes where the violet curve is that from the $Pu_{0.967}Ga_{0.037}$ standard spectrum. The deviations of the spectral amplitudes from the two samples with the highest Ga concentration are seen to be real.

wave from that found in the spectrum of the $Pu_{0.963}Ga_{0.037}$ Pu standard. Inspection of the low k region near the absorption edge of the full spectra (Fig. 11, small upper left figure) does show that there are real differences in the low energy region of the absorption spectra of the different samples. Although those shown are below or at the low end of the phase difference curves in energy and do not necessarily track

the patterns observed in the original spectra, they nevertheless demonstrate that the spectra do vary amongst themselves at low energy as do the phase differences at the beginning of the EXAFS prior to the energies when simple disorder would have a significant effect on the spectra. Such a change could be indicative of expected effects, increasing anharmonicity in the Pu-Pu distribution and an increased amount of Ga phase shift since a Ga neighbor is not being included in the fit. These could continuously alter the Pu-Pu distances found by curve-fits so that they would find large monotonic changes even where only minimal or small ones are actually occurring. This phase difference analysis, however, helps to separate real changes in distance from these other influences.

The trends with Ga concentration observed in the FT moduli are corroborated in the relative numbers of atoms found by taking the logarithm of the amplitude ratios of the nearest neighbor shell (Fig. 11, lower). Relative to the amplitude from the spectrum of $Pu_{0.963}Ga_{0.037}$ that was used as a standard, the numbers of Pu atoms in this shell are $(80 \pm 1)\%$, $(79 \pm 1)\%$, $(69 \pm 1)\%$, $(108 \pm 6)\%$, and $(95 \pm 8)\%$ as much for, respectively, $Pu_{0.983}Ga_{0.017}$, $Pu_{0.977}Ga_{0.023}$, $Pu_{0.970}Ga_{0.030}$, $Pu_{0.953}Ga_{0.047}$, and $Pu_{0.935}Ga_{0.065}$ samples. Quantified by this method, the sample with the lowest Ga concentration that exhibits σ' and the next lowest $Pu_{0.977}Ga_{0.023}$ sample that is a mixture of δ and the σ structure have very similar numbers of atoms in the nearest neighbor shell that are significantly— around 20%—reduced from those of the $Pu_{0.963}Ga_{0.037}$ standard. This value drops an additional 10% at the next composition increment, $Pu_{0.970}Ga_{0.030}$. The samples with higher Ga concentrations above the $\sim$3.3 at. % Ga σ boundary display larger numbers of neighbor atoms, possibly even slightly exceeding that of the standard before the reduction continues because of anharmonicity and other effects. They also exhibit larger Debye-Waller factors, within the range of earlier reports [25,35,37], supporting the importance of local elastic effects and the heterogeneity as a means of ameliorating local stress. These results are consistent with and supportive of the δ $Pu_{30}Ga$-σ/σ' model proposed for δ-stabilized Pu-Ga. The numbers of atoms in the Pu nearest neighbor δ shell should be lower when the δ fraction of the material is depleted because some of the Pu atoms are in the σ/σ' structures. A smaller Debye-Waller factor for the nearest neighbor Pu-Pu pair would be expected below saturation when the $Pu_{30}Ga$ forms with minimal or negligible numbers of extra Ga atoms that strain its structure. The logarithm-amplitude ratio analysis (Fig. 11, lower) shows that the Debye-Waller factors for $Pu_{0.983}Ga_{0.017}$, $Pu_{0.977}Ga_{0.023}$, and $Pu_{0.970}Ga_{0.030}$ are, respectively, -0.0014 ± 0.001, -0.0013 ± 0, and -0.0009 ± 0 Å^2 lower than that of the $Pu_{0.963}Ga_{0.037}$ standard. A higher Debye-Waller factor occurs above saturation because of this strain, and this same analysis does give differences in the Debye-Waller factors relative to the standard of 0.0010 ± 0.002 and 0.0019 ± 0.003 Å^2 for $Pu_{0.953}Ga_{0.047}$ and $Pu_{0.935}Ga_{0.065}$, respectively. The 15% lower number of Pu nearest neighbors with respect to the Ga for $Pu_{0.983}Ga_{0.017}$ is consistent with the model whereby Ga is incorporated within the larger σ' but not the smaller σ domains in a disordered way that makes minimal contributions to the spectrum that overlaps with the nearest neighbor one being analyzed. The exception is the number of Pu-Pu nearest neighbors for $Pu_{0.977}Ga_{0.023}$. This is lower than

the preceding sample whereas it would be expected to be higher as the number of δ Pu atoms increases with diminished σ. This shell of atoms becomes less ordered as the amount of $\delta/Pu_{30}Ga$ increases, and the σ fraction decreases with increasing Ga concentration prior to saturation.

Understanding this ostensible contradiction requires a deeper understanding of the relationship between the EXAFS and the structure. For the long-range average structure of σ to be *Fm3m* with a lattice parameter of 4.95–5.00 Å, the ordered Pu shell at 3.8 Å that is diagnostic for σ must be balanced by a distribution of Pu atoms at around 3.2 Å so that the average position is just above 3.5 Å. Since no additional non-δ distances were observed, this σ shell must either not be resolved from the δ one—which would be the case at this distance—or its own contribution to the EXAFS must be small because its distribution is far from Gaussian. Depending on the size of any peaks in this distribution and their separation(s) from the δ Pu-Pu distance, the contribution of this shorter σ shell to the EXAFS could interfere either constructively with the signal from the δ Pu nearest neighbor shell to increase the amplitude of the peak, destructively to reduce it, or have little or no effect. This is in addition to the loss of amplitude caused by the reduced number of δ Pu atoms. That the EXAFS amplitude is reduced without a concomitant increase in the Debye-Waller factor means that the separation(s) of the peaks in the distributions must be large enough to cause destructive interference between the δ and σ waves, imposing a constraint on the arrangement of these atoms in the σ structure. Under these conditions even small changes in these separations can have large effects on the total amplitude. The most likely explanation, consistent with the types of changes that cause the shifting between the σ and σ' structures, is that the variation in the size and number of the σ domains affects their interaction with the host δ lattice and modifies the distribution of Pu atoms in this shell of atoms that is most strongly coupled to the δ host via direct bonding. This would also be consistent with the suggestion that the modulation of the σ structure is largely to facilitate the formation of such bonds.

This interpretation of the Pu phase differences as showing no real change in distance but rather changes in the phase originating in some combination of disorder and increased numbers of Ga neighbors is supported by those for the Ga-Pu (Fig. 12, center). The Ga-Pu phase differences do not show any significant departures from horizontal over the entire concentration range while the changes of -0.004 ± 0.002, -0.001 ± 0, and -0.006 ± 0.001 Å relative to the $Pu_{0.953}Ga_{0.047}$ standard for, respectively, $Pu_{0.983}Ga_{0.017}$, $Pu_{0.970}Ga_{0.030}$, and $Pu_{0.935}Ga_{0.065}$ that are not correlated with the Ga concentration are negligible. The similarities in the shapes of the phase differences and their small deviations from horizontal occur despite differences in the original absorption spectra at very low energy (Fig. 12, small upper left figure), suggesting that the separation of the phase from the spectra and subsequent subtraction remove simple differences so that those observed are most likely real. The Ga-Pu phase differences at 90 K (Fig. 12, center, small symbols) show that, apart from the deviations from the lines, the cumulative error in the complete process can be as high as around 0.01 Å, well over any temperature driven expansions in the bond lengths. The results at higher temperature also
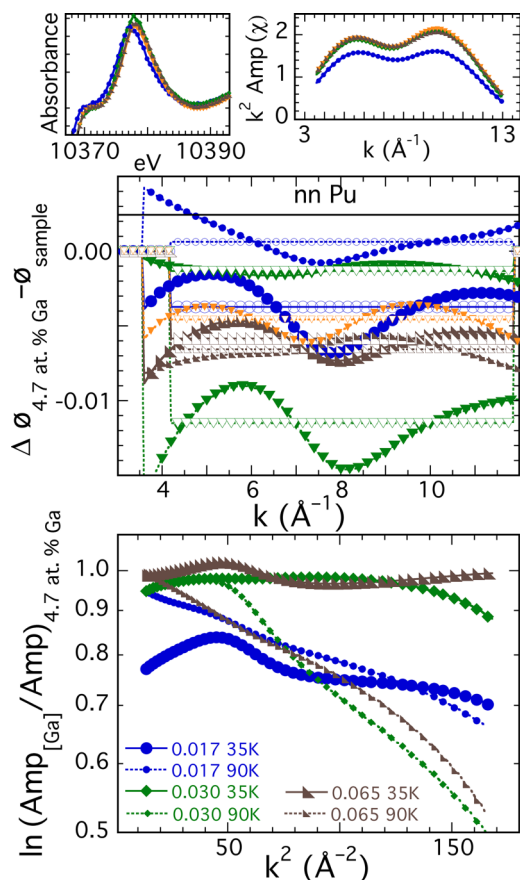
FIG. 12. (Color online) As in Fig. 11, but for Ga-Pu instead of Pu-Pu and including the amplitude ratios at 90 K as well as 35 K to show the change in the thermal component of the Debye-Waller factor. Solid lines utilize 35 K Ga spectra, dashed lines are for 90 K, but all calculations utilize the standard at 35 K. (Blue circles are for $Pu_{0.983}Ga_{0.017}$, green diamonds are for $Pu_{0.970}Ga_{0.030}$, brown left-facing triangles are for $Pu_{0.935}Ga_{0.065}$, downward-pointing triangles in the upper two plots are for the $Pu_{0.953}Ga_{0.047}$ standard, with large symbols representing the 35 K data, small symbols the 90 K data, filled symbols the data, and open symbols the fits to the horizontal lines.) (Center) Phase differences of nearest neighbor δ Ga-Pu wave between spectra of indicated Pu-Ga samples and that of the $Pu_{0.953}Ga_{0.047}$ used as a standard and the fits to expected horizontal line that is the basis for the listed results. The small upper left figure shows the absorption spectra over the white line of the edge region. Although the original spectra exhibit some differences in this region, they do not cause substantial deviations from the expected functional form of the phase difference. (Lower) Logarithmic plot of amplitude ratio for the same spectral components; the listed results are from a linear fit to the ln-ratio where the intercept gives the relative number of atoms in this shell and the slope gives the change in the Debye-Waller factor. The small upper right figure contains the amplitude envelopes. The ratios show the expected increase in the Debye-Waller factor with temperature. However, the negative slopes of these curves also result in their projection at zero to higher numbers of atoms, which is incorrect.

demonstrate, as do the Pu data at 90 K that are not shown here [37], that at least over this range there is no significant temperature dependence of the bond lengths. The different temperatures at which the two sets of measurements were made

cannot be the source of the discrepancy between this analysis and previous reports anyway. The Invar effect [30,82,83] in δ PuGa, whereby the thermal contraction increases with increasing Ga concentration, could enhance the shortening of the bond lengths with higher amounts of Ga. The issue of deviations from Vegard's law in δ Pu-Ga that are >0.02 Å for materials with more than 6 at. % Ga therefore remains largely unanswered because of the limited composition range of these samples.

The logarithm-amplitude ratios of the Ga spectra (Fig. 12, lower) give relative numbers of Pu atoms in the first shell relative to the standard of $(85 \pm 2)\%$, $(98 \pm 1)\%$, and $(102 \pm 1)\%$ for, respectively, $Pu_{0.983}Ga_{0.017}$, $Pu_{0.970}Ga_{0.030}$, and $Pu_{0.935}Ga_{0.065}$. The corresponding changes in the static components of the Debye-Waller factors at 35 K are 0.006 ± 0, 0 ± 0, and -0.002 ± 0.001 Å^2. As with the Pu, these mostly recapitulate $\chi(R)$ with the refinement of attaching quantities to the trends. A 15% reduction in the number of neighbor Pu atoms for $Pu_{0.983}Ga_{0.017}$ and a slightly increased Debye-Waller factor occur for the sample that contains the σ' structure, but constant numbers and Debye-Waller factors are found for the other two samples. This analysis also shows the expected increases in the Debye-Waller factors when the temperature is elevated to 90 K.

I. The contraction around the Ga atoms and collective, many-body mechanisms for the Vegard's law type bulk lattice contraction

Consistent with a preference for forming $Pu_{30}Ga$ that would preclude element-specific interactions between atoms, deviations from Vegard's law type behavior do not occur as a function of composition in these samples. Nevertheless there is a departure that is of perhaps greater interest. Comparing the Pu and Ga curve-fitting results (Table I), $\Delta R_{\text{nearest neighbor}}$ (Pu-Pu) $-$ (Ga-Pu) for $Pu_{0.983}Ga_{0.017}$, $Pu_{0.970}Ga_{0.030}$, $Pu_{0.943}Ga_{0.047}$, and $Pu_{0.935}Ga_{0.065}$ are, respectively, almost constant at 0.121, 0.118, 0.121, and 0.119 Å. Under the assumption of Vegard's law that this volume difference propagates to all distances, the expected contraction around Ga for the third neighbor shell at 5.68 Å that holds 24 atoms—accounting for its large contribution to the spectra—is 0.039 Å. What is found instead are 0.026, 0.022, 0.021, and 0.002 Å. Since these are relative values, errors in the calculated phase shifts that would affect the absolute results cancel so that these differences of around 0.02 Å from the calculation are significant. Thus the Ga-centered contraction is relaxing too quickly and would not extend to infinity as assumed. This raises the question of what is the mechanism for the bulk contraction?

The answer is again found in—and helps corroborate—the invariance of the Ga EXAFS across the composition range. We define the local strain field as the Pu atoms around a Ga that are displaced towards the smaller Ga relative to their positions with respect to a central Pu. A conflict occurs when two Ga atoms are in sufficient proximity that their local strain fields overlap. The common atoms are pulled in both directions (Fig. 13, upper left). The expectation is that they would move to a compromise position that would disorder the Ga $g(r)$ as the Ga concentration and the number of such Ga
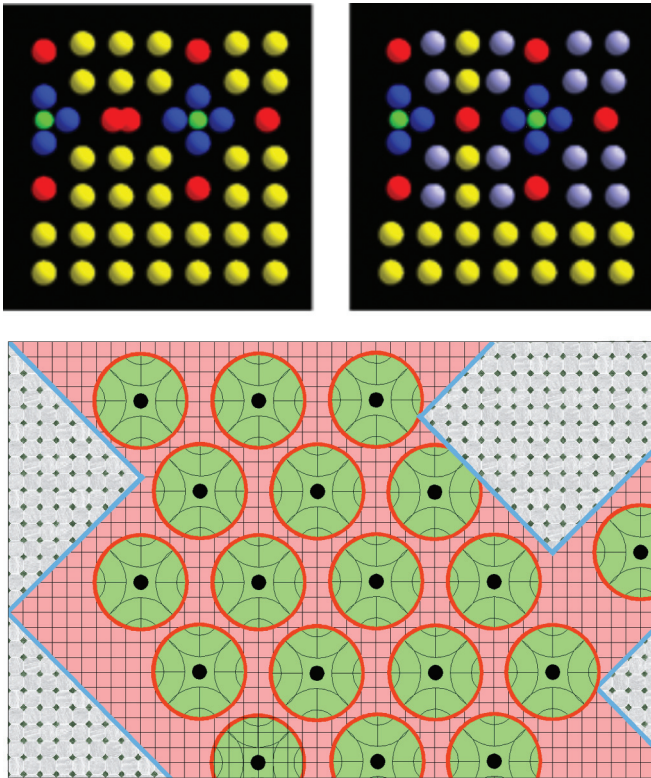
FIG. 13. (Color) (Upper) A many-body mechanism for Vegard's law type behavior suggested by the invariance of the Ga environments results when the Pu atoms in the local strain field (blue and red) around the Ga atoms (green) overlap because of the proximity of two Ga's, so that those contained in both strain fields are pulled in two directions (right). In order to conserve the Ga environment the material responds by displacement of the two locally strained regions towards each other, displacing a stripe of adjacent Pu atoms (purple) with them along the Ga-Ga vector. The overlap of these stripes to produce networks extending through the entire crystal gives the bulk contraction. (Lower) The results presented in this paper are summarized in this schematic depiction of metastable (Ga concentration $\leq$3.3 at. %) δ Pu-Ga alloy. The contraction around the smaller Ga atom (black) creates a local strain field (green) of finite size (red circle, ~11.6 Å) around each one. The interactions of these strain fields with each other and with the lattice cause the Ga atoms to self-organize into domains of composition $Pu_{25-35}Ga$ dictated by these strain fields being in contact with but not overlapping each other. These domains (pink) exhibit the fcc δ structure. A consequence of this self-organization is the presence of Ga-depleted domains (gray and green) that, if isolated, would be in the α phase. However, their association with the δ Pu exerts tensile or negative pressure on them, causing them to rearrange into a second, low density, modulated, ordered structure that we have named σ, resulting in nanoscale heterogeneity, i.e., the coexistence of two ordered structures within the same crystal. Continuous percolation paths connecting the δ domains are the origin of the Vegard's law type behavior, i.e., the linear contraction of the lattice with increasing Ga concentration.

pairs and triplets increases, causing the amplitudes in the Ga EXAFS to diminish, faster at higher R, but this effect is not observed; the amplitudes are the same in all of the spectra. Alternatively, if the Ga environments are rigid inside of a much softer set of Pu atoms, then the Ga atoms can maintain the positions of their neighbors if they move towards each other (Fig. 13, upper right). In doing so, they pull a "stripe" of Pu atoms aligned along the Ga-Ga displacement vector along with them, with smaller displacements farther from the vector. These stripes are sufficiently large so that they overlap to form a continuous, contracted network that extends through the entire crystal even at low Ga concentrations. Remarkably, calculations of this effect (not shown here) demonstrate that this contraction is linear with Ga concentration up through 8–10 at. % Ga; the mechanics of the stripe formation and crystal contraction in concert with the probability of Ga pairs and higher order combinations give bulk behavior that is close to linear. Deviations from the Vegard's law line can be induced by changing the probability of Ga combinations from random, by having Ga atoms attract (although longer range and never to form Ga-Ga bonds) or repel each other, consistent with our proposal for the $Pu_{30}Ga$ quasi-intermetallic. Thus, at least over limited concentration ranges, Vegard's law type behavior can be caused by a collective, many-body effect.

IV. CONCLUDING REMARKS

The starting point in understanding δ Pu-Ga is acknowledging that mean-field approaches in which the Ga and Pu atoms average into a uniform composite are invalid. The combined XAFS/XRD/PDF experiments reported here clearly demonstrate the strength of a local approach in which the different elements effectively retain their particular disparate identities. We discuss the consequences of this here; the fact that the presence of strongly interacting inhomogeneities can cause them to aggregate and self-organize to produce a nanoscale phase-separated material whose signatures are more apparent in local structure than diffraction and other measurements but should nevertheless affect them, the association of elastic strain with such a two-state system, the coupling of elastic strain and phase stability to the electronic structure, and finally the importance of these structural properties of Pu vis-à-vis martensitic materials and properties and ultimately other complex correlated materials.

The second point in understanding δ Pu-Ga is that after localization collective and cooperative effects are central. The Ga atoms with their own characteristics interact strongly enough to self-organize at ~5.6 Å separations. The evidence is that they never form direct bonds—which may explain the upper Ga concentration limit for δ Pu in the phase diagram—but at longer distances, they attract each other to form a quasi-intermetallic even though this results in regions where the local Ga concentration is effectively zero [64]. In these Ga-depleted regions, however, the interactions of the Pu atoms with each other are now strong enough so that, under the constraint of being embedded in the δ Pu host, domains of dozens to hundreds of atoms that sum up to as much as 20% of the crystal rearrange into a novel structure (Fig. 13, lower). The material is therefore heterogeneous—containing multiple ordered structures—on the nanometer scale at or below the diffraction limit. Addressing the putative contradiction in this concept, that a material could contain tens of percents of a second ordered structure that would not give an unambiguous signal in diffraction, delayed detailed reporting of these results

[20,21] while we undertook an extensive evaluation of local order and heterogeneity [38–41,43,44], ultimately finding that this type of behavior was easily produced because of the limitations of crystallography. Arguing this attribute of the structure by claiming that, for example, scattering, photoemission, microscopy, and ultrasound data contradict it ignores the fact that all experimental methods are limited to their intrinsic length and timescales. Thus, the suggestions of structural and transformational complexity that have transpired indirectly from photoemission [11,13,22,84], diffraction [23], phonon spectra [55,85–87], the identification of the instabilities of some of the structures along the Bain paths that connect them [88–90], and even heat capacity measurements that have assigned the anomalous behavior of δ Pu alloys to the structural phenomena [49,50] can be viewed as the signatures of the individual and collective lattice distortions found in the local structure measurements. Local structure results are complementary to methods that are sensitive to the average properties of a large number of atoms or to the periodic or coherent portions of a material, so that such putative contradictions are most likely to be indicative of essential components of the structure:property relationships. Perhaps the most important example is the anomalous elastic softness that has been identified as a bulk property of the elastic moduli by resonance ultrasound [88,91,92], in particular aspects of the phonon dispersion curves [85,86,93]—some of which differ from calculations [89], and as anisotropic atomic displacements in diffraction [23].

The importance of elastic strain in δ Pu begins at the bulk scale, where it exhibits the highest strain anisotropy of any fcc metal [88,92,93]. Significant hysteresis in the phase transition of ultrapure Pu has recently been reported [31]. In Pu-Ga, instead of being either abrupt or continuous (as it is on cooling) the $\alpha' \rightarrow \delta$ transformation that occurs when a polycrystalline Pu-Ga sample at lower Ga concentrations is heated from low temperatures occurs as a series of periodic bursts, presumably because it is triggered by stress that accumulates throughout the entire mass of material [28]. Elastic stress also determines the geometry of the grains in these mixtures [27,30]. These effects propagate below the diffraction limit where, analogous or possibly identical to this report, it has been suggested that nanodomains of an α'-like material can form [23,29] and that the surface of α Pu reconstructs into a more δ-like structure (possibly related to the σ structure we have found here) in response to the elastic and electronic anisotropy [22]. Within δ Pu and its alloys, direct measurements of the elastic moduli show an unusual and in some respects unique softness at higher temperatures that is very difficult to reconcile with its negative-to-flat thermal expansion coefficient [91]. An Invar-type two-level model has been proposed to account for these properties [82,83,91], with the suggestion that the high energy/low volume states might be related to the local cluster around Ga because the thermal expansion coefficient becomes positive at low temperatures even at 2 at. % Ga and then positive throughout with more Ga [83]. It was, however, also pointed out that certain types of electronic structure calculations find two levels intrinsically [8,14,84,94] with one suggestion that the second level possesses an electronic structure like that of ε Pu [95] which is connected to δ Pu by a soft, Bain transformation [55,85,86,88,90,91,93,96]. This

multilevel approach for Pu in compounds as well as pure metal has also received substantial experimental corroboration [11,12,15,97]. These local structure results corroborate the idea that the anomalous elastic behavior is pervasive down to the atomic level [23] in terms of unusual flexibility in the ways in which the atoms can arrange themselves, but beyond that it is difficult to find any correlations with these predictions. Although the σ/σ' heterogeneity with the δ structure is a part of the Pu-Ga energy landscape even for higher Ga concentrations where it would be latent rather than realized, its characteristics are not similar to those of the projected Invar state or to the ε phase (likewise the local environment around the Ga sites nor is there any indication of a second state or any structural heterogeneity for Ga concentrations >3.3 at. %. Insofar as the Invar model assumes that there are no local phonons to contribute vibrational entropy and the heterogeneity will itself make its own contributions that would not occur in a homogeneous material, these findings complicate the interpretation that other types of results point to Invar-type behavior. If anything, they suggest that the effect of the alloy elements may simply be to counteract the anomalies that accrue to Pu so that the alloys are simply more like normal metals.

The elastic response and the associated structural transformations—both in the phase diagram and the local ones described here—are extreme because of the narrowness of the f bands and the fact that the f electrons are ambivalent, occupying both localized and itinerant bonding states [11,22] with the former favored at Pu because of a strong spin-orbit interaction [10,98,99]. These characteristics contribute to the unusually strong electron-phonon coupling [9] that is the origin of the sensitivity of Pu and its alloys to transformation [55]. The feedback between displacements of the atoms in real space and the electronic hybridization and highly directional bonding in momentum space [98] that result in the unusually high anisotropic responses to strain [23,58,65,88,91,92] undoubtedly contribute significantly to the problems with reaching a consensus on the electronic and crystal structures of Pu and its alloys. Thus, whereas the long-range average bulk homogeneous properties away from transformations are calculated accurately [85,86,89,100,101], it has been noted that the soft modes in the phonon spectra are more problematic [91,92]. Perhaps because it has proven so intractable, δ Pu already has an unfortunate history of theories [96,102,103] expounded in defiance of experimental results [104]. Even with the renewed consensus that the experimental absence of magnetism is correct [12,13,105,106], there is still disagreement on the best approach to the δ Pu problem, with proponents of working harder to refine the parameters used in conventional descriptions [105,106] maintaining their positions in opposition to more unusual approaches such as anisotropic bonding [58] and admixtures of quantum states [14,84]. The results presented here only serve at this time to amplify the conflict between experiment and theory; none of the current theories include the observed localization of the structural properties or even the possibility of novel structures and heterogeneity. Multiple, coexisting structures will also affect the entropy [9,83] as well as signifying that the systems studied may not be at thermodynamic equilibrium. This is regrettable for Pu insofar as it has resulted in the

technologically critical aging issue being solved by analogies with more conventional materials that predict one to two orders of magnitude fewer radiation-induced defects than actually occur because of stabilization by interacting with themselves or other inhomogeneities [20,21,37].

The simplest interpretation of the heterogeneous $\delta-\sigma$ Pu alloy structure is that it is the finest scale "texture," i.e., the smallest manifestation of the fine tweed-coarse tweed-twin progression that accompanies the transformation in martensitic and related materials [62]. Analogous to the behavior of Pu just described, fine-scale texture is often observed well in advance of the actual transition and is not necessarily coupled to observable changes in the static, macroscopic materials properties.

These results demonstrate the inverse coupling between the scale and width of the transformation in δ Pu alloys, such that on this nanometer scale, the transformation range is so large that the transition remains incomplete at finite temperature. The other implied scaling relationship pertains to the materials properties, since the only known difference between stable/homogeneous δ and metastable/heterogeneous $\delta-\sigma$ Pu alloys is the propensity of the latter to transform to the α phase. Attributes such as hardness that depend upon the average behavior of all of the atoms over microns are apparently unaffected by nanoscale structure, whereas phase stability issues that originate in nucleation phenomena involving collective behavior of only a small number of atoms do show sensitivity to small length scales. Thus, on the local scale, the martensitic transformation mechanism may differ from that involving larger ones [55]. In metastable δ Pu-Ga, 20% of the material is structured to exhibit α-like characteristics, suggesting that the transformation should proceed simply by connecting these domains and making it difficult to understand how nucleation can be the rate limiting step. The relationship between scale and symmetry is also important. An argument against the heterogeneity is its absence in transmission electron microscopy (TEM) images [27]. This, however, neglects to account for the anisotropy of the strain field in the ultrathin TEM sample that allows for facile relaxation along the transmission axis. Thin sections and surfaces may be intrinsically incompatible with the identification and characterization of effects related to microscopic elastic response; after all, the oxide that must be on the surface is not normally reported in TEM measurements.

We have recently suggested that a dynamic energy landscape utilizing the possible local conformations of the atoms in terms of the numbers and locations of the inhomogeneities in their environments and the shifting of the energies of the competing conformations in response to these environments may be the best approach to modeling complex materials, including Pu, on the atomic scale [37]. This would also include, consistent with recent linear discriminant analysis-dynamical mean field theory (LDA-DMFT) calculations [13,14], the ability of the atoms to shift between different states so that, in certain configurations or local compositions, groups of atoms could lower their energy by rearranging, which would result in and be the origin of heterogeneity. In such an energy landscape, conformations that are higher in energy for a given set of conditions would be latent as a local minimum in the unoccupied higher energy regions of the landscape. Bulk properties such as the hardness would therefore be continuous because they

traverse identical or at least very similar landscapes even as the composition and local structure change.

Nanometer-scale texture is an attribute of many complex materials of current interest that exhibit interesting correlated and phase stability properties. The "stripes" in cuprate superconductors [107,108], manganite colossal magnetoresistance (CMR) compounds [109], and related transition metal oxides [110], as well as nondiffracting ordered domains in magnetic alloys [42,111] appear to be coupled to the unusual or unique correlated and transformational properties of these types of compounds. Metastable δ Pu-Ga resembles the latter, displaying static chemical ordering, rather than the first set where the stripes are associated with dynamic ordering of charge and spin. Including metastable δ Pu alloys within the class of complex materials will assist in understanding it while also enhancing our understanding of complexity. These alloys reinforce the view that nanometer-scale heterogeneity is an important characteristic of complex materials, even in ones with very simple formulas and crystallographic behavior. They also emphasize the importance of both short- and long-range elastic forces in addition to electronic structure as critical components of structure and properties [74,112,113].

There remain two experimental challenges that are consequences of these collective and cooperative effects and resulting nanoscale heterogeneity that must be resolved in the future to complete this work: (1) on the angstrom to nanometer scale, what is the arrangement of the atoms in the σ structure; and (2) on the scale of a few to several nanometers, how are the σ domains arranged to account for the tremendous variability in the intensities of their diffraction patterns in different samples? The origins of these phenomena in the electronic structure are a separate problem, but also one that could be expected to help resolve the current issue of the most accurate description of the $5f$ states.

[1] J. L. Smith and E. A. Kmetko, J. Less Common Met. **90**, 83 (1983).

[2] N. G. Cooper, in *Los Alamos Science*, edited by N. G. Cooper (Los Alamos National Laboratory, Los Alamos, New Mexico, 2000), Vol. 26, pp. 493.

[3] G. H. Lander, Science **301**, 1057 (2003).

[4] S. S. Hecker, Metall. Trans. A **35**, 2207 (2004).

[5] S. S. Hecker, D. R. Harbur, and T. G. Zocco, Prog. Mat. Sci. **49**, 429 (2004).

[6] A. J. Schwartz, J. Alloys Compd. **444-445**, 4 (2007).

[7] L. Nordström, J. M. Wills, P. H. Andersson, P. Söderlind, and O. Eriksson, Phys. Rev. B **63**, 035103 (2000).

[8] S. Y. Savrasov, G. Kotliar, and E. Abrahams, Nature **410**, 793 (2001).

[9] M. J. Graf, T. Lookman, J. M. Wills, D. C. Wallace, and J. C. Lashley, Phys. Rev. B **72**, 045135 (2005).

[10] J. G. Tobin, K. T. Moore, B. W. Chung, M. A. Wall, A. J. Schwartz, G. van der Laan, and A. L. Kutepov, Phys. Rev. B **72**, 085109 (2005).

[11] J. J. Joyce, J. M. Wills, T. Durakiewicz, M. T. Butterfield, E. Guziewicz, D. P. Moore, J. L. Sarrao, L. A. Morales, A. J. Arko, O. Eriksson, A. Delin, and K. S. Graham, Physica B **378–380**, 920 (2006).

[12] J. G. Tobin, P. Soderlind, A. Landa, K. T. Moore, A. J. Schwartz, B. W. Chung, M. A. Wall, J. M. Wills, R. G. Haire, and A. L. Kutepov, J. Phys. Condens. Matter **20**, 125204 (2008).

[13] J. X. Zhu, A. K. McMahan, M. D. Jones, T. Durakiewicz, J. J. Joyce, J. M. Wills, and R. C. Albers, Phys. Rev. B **76**, 245118 (2007).

[14] J. H. Shim, G. Kotliar, and K. Haule, Nature **446**, 513 (2007).

[15] C. H. Booth, Y. Jiang, D. L. Wang, J. N. Mitchell, P. H. Tobash, E. D. Bauer, M. A. Wall, P. G. Allen, D. Sokaras, D. Nordlund, T. C. Weng, M. A. Torrez, and J. L. Sarrao, Proc. Natl. Acad. Sci. USA **109**, 10205 (2012).

[16] D. L. Clark, S. S. Hecker, G. D. Jarvinen, and M. P. Neu, in *The Chemistry of the Actinide and Transactinide Elements*, 3rd ed., edited by L. R. Morss, N. M. Edelstein, J. Fuger, and J. J. Katz (Springer, Netherlands, 2006), pp. 813.

[17] S. Drell, R. Jeanloz, and B. Peurifoy, Science **283**, 1119 (1999).

[18] R. Jeanloz, Phys. Today **53**, 44 (2000).

[19] O. J. Wick, *Plutonium Handbook: a Guide to the Technology* (American Nuclear Society, La Grange Park, IL, 1980), pp. 966.

[20] S. D. Conradson, Appl. Spectrosc. **52**, 252A (1998).

[21] S. D. Conradson, in *Challenges in Plutonium Science*, edited by N. G. Cooper (Los Alamos National Laboratory, Los Alamos, New Mexico, 2000), Vol. 26, pp. 356.

[22] L. Havela, T. Gouder, F. Wastin, and J. Rebizant, Phys. Rev. B **65**, 235118 (2002).

[23] A. C. Lawson, J. A. Roberts, B. Martinez, R. B. Von Dreele, B. Storey, H. T. Hawkins, M. Ramos, F. G. Hampel, C. C. Davis, R. A. Pereyra, J. N. Mitchell, F. Freibert, S. M. Valone, T. N. Claytor, D. A. Viskoe, and F. W. Schonfeld, Philos. Mag. **85**, 2007 (2005).

[24] C. Platteau, P. Bruckel, B. Ravat, and F. Delaunay, J. Nucl. Mater. **385**, 108 (2009).

[25] C. H. Booth, Y. Jiang, S. A. Medling, D. L. Wang, A. L. Costello, D. S. Schwartz, J. N. Mitchell, P. H. Tobash, E. D.

[ ] Bauer, S. K. McCall, M. A. Wall, and P. G. Allen, J. Appl. Phys. **113**, 093502 (2013).

[26] Y. M. Jin, Y. U. Wang, A. G. Khachaturyan, C. R. Krenn, and A. J. Schwartz, Metall. Mater. Trans. A **36**, 2031 (2005).

[27] T. G. Zocco and A. J. Schwartz, JOM **55**, 24 (2003).

[28] K. J. M. Blobaum, C. R. Krenn, J. N. Mitchell, J. J. Haslam, M. A. Wall, T. B. Massalski, and A. J. Schwartz, Metall. Trans. A **37**, 567 (2006).

[29] K. J. M. Blobaum, C. R. Krenn, M. A. Wall, T. B. Massalski, and A. J. Schwartz, Acta Mater. **54**, 4001 (2006).

[30] J. P. Hirth, J. N. Mitchell, D. S. Schwartz, and T. E. Mitchell, Acta Mater. **54**, 1917 (2006).

[31] T. G. Zocco, D. S. Schwartz, and J. Park, J. Nucl. Mater. **353**, 119 (2006).

[32] L. E. Cox, R. Martinez, J. H. Nickel, S. D. Conradson, and P. G. Allen, Phys. Rev. B **51**, 751 (1995).

[33] P. Faure, B. Deslandes, D. Bazin, C. Tailland, R. Doukhan, J. M. Fournier, and A. Falange, J. Alloys Compd. **244**, 131 (1996).

[34] N. Richard, P. Faure, P. Rofidal, J. L. Truffier, and D. Bazin, J. Alloys Compd. **271–273**, 879 (1998).

[35] P. G. Allen, A. L. Henderson, E. R. Sylwester, P. E. A. Turchi, T. H. Shen, G. F. Gallegos, and C. H. Booth, Phys. Rev. B **65**, 214107 (2002).

[36] E. J. Nelson, K. J. M. Blobaum, M. A. Wall, P. G. Allen, A. J. Schwartz, and C. H. Booth, Phys. Rev. B **67**, 224206 (2003).

[37] S. D. Conradson, N. Bock, J. M. Castro, D. R. Conradson, L. E. Cox, W. Dmowski, D. E. Dooley, T. Egami, F. J. Espinosa-Faller, F. Freibert, A. J. Garcia-Adeva, N. J. Hess, E. Holmström, R. C. Howell, B. A. Katz, J. C. Lashley, R. J. Martinez, D. P. Moore, L. A. Morales, J. D. Olivas *et al.*, J. Phys. Chem. C **118**, 8541 (2014).

[38] D. A. Dimitrov, A. L. Ankudinov, A. R. Bishop, and S. D. Conradson, Phys. Rev. B **58**, 14227 (1998).

[39] D. A. Dimitrov, A. R. Bishop, and S. D. Conradson, Phys. Rev. B **56**, 2969 (1997).

[40] S. D. Conradson, F. J. Espinosa, A. Henderson, and P. M. Villella, in *International Symposium on Physics in Local Lattice Distortions (LLD2K)*, edited by H. Oyanagi and A. Bianconi (AIP, Tsukuba, Japan, 2000), Vol. 554, pp. 503.

[41] A. J. Garcia-Adeva, D. R. Conradson, P. Villella, and S. D. Conradson, J. Phys. Chem. B **107**, 6704 (2003).

[42] F. J. Espinosa-Faller, R. C. Howell, A. J. Garcia-Adeva, S. D. Conradson, A. Y. Ignatov, T. A. Tyson, R. F. C. Farrow, and M. F. Toney, J. Phys. Chem. B **109**, 10406 (2005).

[43] R. C. Howell, S. D. Conradson, and A. J. Garcia-Adeva, J. Phys. Chem. B **111**, 159 (2007).

[44] D. A. Andersson, L. Casillas, M. I. Baskes, J. S. Lezama, and S. D. Conradson, J. Phys. Chem. B **113**, 11965 (2009).

[45] J. C. Lashley, M. S. Blau, K. P. Staudhammer, and R. A. Pereyra, J. Nucl. Mater. **274**, 315 (1999).

[46] M. Dormeval, C. Valot, and N. Baclet, J. Phys. IV **10**, 425 (2000).

[47] M. Dormeval, N. Baclet, C. Valot, P. Rofidal, and J. M. Fournier, J. Alloys Compd. **350**, 86 (2003).

[48] J. E. Lynn, G. H. Kwei, W. J. Trela, V. W. Yuan, B. Cort, R. J. Martinez, and F. A. Vigil, Phys. Rev. B **58**, 11408 (1998).

[49] J. C. Lashley, A. Migliori, J. Singleton, R. J. McQueeney, M. S. Blau, R. A. Pereyra, and J. L. Smith, JOM **55**, 34 (2003).

[50] J. C. Lashley, J. Singleton, A. Migliori, J. B. Betts, R. A. Fisher, J. L. Smith, and R. J. McQueeney, Phys. Rev. Lett. **91**, 205901 (2003).

[51] S. D. Conradson, B. D. Begg, D. L. Clark, C. den Auwer, M. Ding, P. K. Dorhout, F. J. Espinosa-Faller, P. L. Gordon, R. G. Haire, N. J. Hess, R. F. Hess, D. W. Keogh, L. A. Morales, M. Neu, P. Paviet-Hartmann, W. Runde, C. D. Tait, D. K. Veirs, and P. M. Villella, J. Am. Chem. Soc. **126**, 13443 (2004).

[52] S. D. Conradson, D. Manara, F. Wastin, D. L. Clark, G. H. Lander, L. A. Morales, J. Rebizant, and V. V. Rondinella, Inorg. Chem. **43**, 6922 (2004).

[53] A. L. Ankudinov, B. Ravel, J. J. Rehr, and S. D. Conradson, Phys. Rev. B **58**, 7565 (1998).

[54] F. H. Ellinger, C. C. Land, and V. O. Struebing, J. Nucl. Mater. **12**, 226 (1964).

[55] R. Q. Xu, J. Wong, P. Zschack, H. Hong, and T. C. Chiang, Europhys. Lett. **83**, 26001 (2008).

[56] R. N. R. Mulford, F. H. Ellinger, and K. A. Johnson, J. Nucl. Mater. **17**, 324 (1965).

[57] D. T. Larson and J. M. Haschke, Inorg. Chem. **20**, 1945 (1981).

[58] K. T. Moore, D. E. Laughlin, P. Soderlind, and A. J. Schwartz, Philos. Mag. **87**, 2571 (2007).

[59] J. D. Becker, J. M. Wills, L. E. Cox, and B. R. Cooper, Phys. Rev. B **58**, 5143 (1998).

[60] E. J. Nelson, K. J. M. Blobaum, M. A. Wall, P. G. Allen, A. J. Schwartz, and C. H. Booth, AIP Conf. Proc. **673**, 187 (2003).

[61] N. J. Curro and L. Morales, MRS Symp. Proc. **802**, 53 (2003).

[62] S. Kartha, J. A. Krumhansl, J. P. Sethna, and L. K. Wickham, Phys. Rev. B **52**, 803 (1995).

[63] J. A. Krumhansl, Phase Transit. **69**, 395 (1999).

[64] M. I. Baskes, S. Y. Hu, S. M. Valone, G. F. Wang, and A. C. Lawson, J. Comp.-Aided Mater. Des. **14**, 379 (2007).

[65] K. T. Moore, P. Soderlind, A. J. Schwartz, and D. E. Laughlin, Phys. Rev. Lett. **96**, 206402 (2006).

[66] W. Kuch and S. S. P. Parkin, Europhys. Lett. **37**, 465 (1997).

[67] W. Kuch and S. S. P. Parkin, J. Magn. Magn. Mater. **184**, 127 (1998).

[68] A. Biedermann, R. Tscheliessnig, C. Klein, M. Schmid, and P. Varga, Surf. Sci. **563**, 110 (2004).

[69] A. Biedermann, R. Tscheliessnig, M. Schmid, and P. Varga, Appl. Phys. A-Mater. **78**, 807 (2004).

[70] B. Horovitz, G. R. Barsch, and J. A. Krumhansl, Phys. Rev. B **43**, 1021 (1991).

[71] S. Kartha, T. Castan, J. A. Krumhansl, and J. P. Sethna, Phys. Rev. Lett. **67**, 3630 (1991).

[72] J. A. Krumhansl, J. Phys. IV **5**, 3 (1995).

[73] A. Saxena, Y. Wu, T. Lookman, S. R. Shenoy, and A. R. Bishop, Physica A **239**, 18 (1997).

[74] S. R. Shenoy, T. Lookman, A. Saxena, and A. R. Bishop, Phys. Rev. B **60**, R12537 (1999).

[75] K. O. Rasmussen, T. Lookman, A. Saxena, A. R. Bishop, R. C. Albers, and S. R. Shenoy, Phys. Rev. Lett. **87**, 055704 (2001).

[76] W. Klein, T. Lookman, A. Saxena, and D. M. Hatch, Phys. Rev. Lett. **88**, 085701 (2002).

[77] C. J. Gagne, H. Gould, W. Klein, T. Lookman, and A. Saxena, Phys. Rev. Lett. **95**, 095701 (2005).

[78] R. Groger, T. Lookman, and A. Saxena, Phys. Rev. B **78**, 184101 (2008).

[79] P. Lloveras, T. Castan, M. Porta, A. Planes, and A. Saxena, Phys. Rev. Lett. **100**, 165707 (2008).

[80] F. J. Espinosa, P. Villela, J. C. Lashley, S. D. Conradson, L. E. Cox, R. Martinez, B. Martinez, L. Morales, J. Terry, and R. A. Pereyra, Phys. Rev. B **63**, 174111 (2001).

[81] U. Scheuer and B. Lengeler, Phys. Rev. B **44**, 9883 (1991).

[82] A. C. Lawson, J. A. Roberts, B. Martinez, J. W. Richardson, H. Ledbetter, and A. Migliori, JOM **55**, 31 (2003).

[83] A. C. Lawson, J. A. Roberts, B. Martinez, M. Ramos, G. Kotliar, F. W. Trouw, M. R. Fitzsimmons, M. P. Hehlen, J. C. Lashley, H. Ledbetter, R. J. McQueeney, and A. Migliori, Philos. Mag. **86**, 2713 (2006).

[84] J. M. Wills, O. Eriksson, A. Delin, P. H. Andersson, J. J. Joyce, T. Durakiewicz, M. T. Butterfield, A. J. Arko, D. P. Moore, and L. A. Morales, J. Electron Spectrosc. Relat. Phenom. **135**, 163 (2004).

[85] J. Wong, M. Krisch, D. L. Farber, F. Occelli, A. J. Schwartz, T. C. Chiang, M. A. Wall, C. Boro, and R. Q. Xu, Science **301**, 1078 (2003).

[86] J. Wong, M. Krisch, D. L. Farber, F. Occelli, R. Xu, T. C. Chiang, D. Clatterbuck, A. J. Schwartz, M. A. Wall, and C. Boro, Phys. Rev. B **72**, 064115 (2005).

[87] M. I. Baskes, A. C. Lawson, and S. M. Valone, Phys. Rev. B **72**, 014129 (2005).

[88] A. Migliori, F. Freibert, J. C. Lashley, A. C. Lawson, J. P. Baiardo, and D. A. Miller, J. Supercon. **15**, 499 (2002).

[89] X. Dai, S. Y. Savrasov, G. Kotliar, A. Migliori, H. Ledbetter, and E. Abrahams, Science **300**, 953 (2003).

[90] T. Lookman, A. Saxena, and R. C. Albers, Phys. Rev. Lett. **100**, 145504 (2008).

[91] A. Migliori, H. Ledbetter, A. C. Lawson, A. P. Ramirez, D. A. Miller, J. B. Betts, M. Ramos, and J. C. Lashley, Phys. Rev. B **73**, 052101 (2006).

[92] A. Migliori, A. Mihut, J. B. Betts, M. Ramos, C. Mielke, C. Pantea, D. A. Miller, and I. Mihut, J. Alloys Compd. **444-445**, 133 (2007).

[93] R. J. McQueeney, A. C. Lawson, A. Migliori, T. M. Kelley, B. Fultz, M. Ramos, B. Martinez, J. C. Lashley, and S. C. Vogel, Phys. Rev. Lett. **92**, 146401 (2004).

[94] G. Kotliar and D. Vollhardt, Phys. Today **57**, 53 (2004).

[95] B. A. Nadykto, J. Alloys Compd. **444-445**, 145 (2007).

[96] P. Soderlind, A. Landa, B. Sadigh, L. Vitos, and A. Ruban, Phys. Rev. B **70**, 144103 (2004).

[97] J. J. Joyce, J. M. Wills, T. Durakiewicz, M. T. Butterfield, E. Guziewicz, J. L. Sarrao, L. A. Morales, A. J. Arko, and O. Eriksson, Phys. Rev. Lett. **91**, 176401 (2003).

[98] K. T. Moore, M. A. Wall, A. J. Schwartz, B. W. Chung, S. A. Morton, J. G. Tobin, J. G. Lazar, F. D. Tichelaar, H. W. Zandbergen, P. Soderlind, and G. van der Laan, Philos. Mag. **84**, 1039 (2004).

[99] K. T. Moore, G. van der Laan, J. G. Tobin, B. W. Chung, M. A. Wall, and A. J. Schwartz, Ultramicroscopy **106**, 261 (2006).

[100] W. A. Harrison, Phys. Rev. B **69**, 113106 (2004).

[101] W. A. Harrison, Phys. Rev. B **69**, 224109 (2004).

[102] P. Söderlind and B. Sadigh, Phys. Rev. Lett. **92**, 185702 (2004).

[103] A. B. Shick, V. Drchal, and L. Havela, Europhys. Lett. **69**, 588 (2005).

[104] J. C. Lashley, A. C. Lawson, R. J. McQueeney, and G. H. Lander, Phys. Rev. B **72**, 054416 (2005).

[105] J. P. Julien, J. X. Zhu, and R. C. Albers, Phys. Rev. B **77**, 195123 (2008).

[106] P. Soderlind, Phys. Rev. B **77**, 085101 (2008).

[107] J. M. Tranquada, B. J. Sternlieb, J. D. Axe, Y. Nakamura, and S. Uchida, Nature **375**, 561 (1995).

[108] A. Bianconi, N. L. Saini, T. Rossetti, A. Lanzara, A. Perali, M. Missori, H. Oyanagi, H. Yamaguchi, Y. Nishihara, and D. H. Ha, Phys. Rev. B **54**, 12018 (1996).

[109] E. Dagotto, T. Hotta, and A. Moreo, Phys. Rep. **344**, 1 (2001).

[110] C.-H. Du, M. E. Ghazi, Y. Su, I. Pape, P. D. Hatton, S. D. Brown, W. G. Stirling, M. J. Cooper, and S. W. Cheong, Phys. Rev. Lett. **84**, 3911 (2000).

[111] T. A. Tyson, S. D. Conradson, R. F. C. Farrow, and B. A. Jones, Phys. Rev. B **54**, R3702 (1996).

[112] A. Bussmann-Holder and A. R. Bishop, Phys. Rev. B **56**, 5297 (1997).

[113] A. Bussmann-Holder, A. Simon, H. Buttner, and A. R. Bishop, Philos. Mag. B **80**, 1955 (2000).